CHALMERS
UNIVERSITY OF TECHNOLOGY

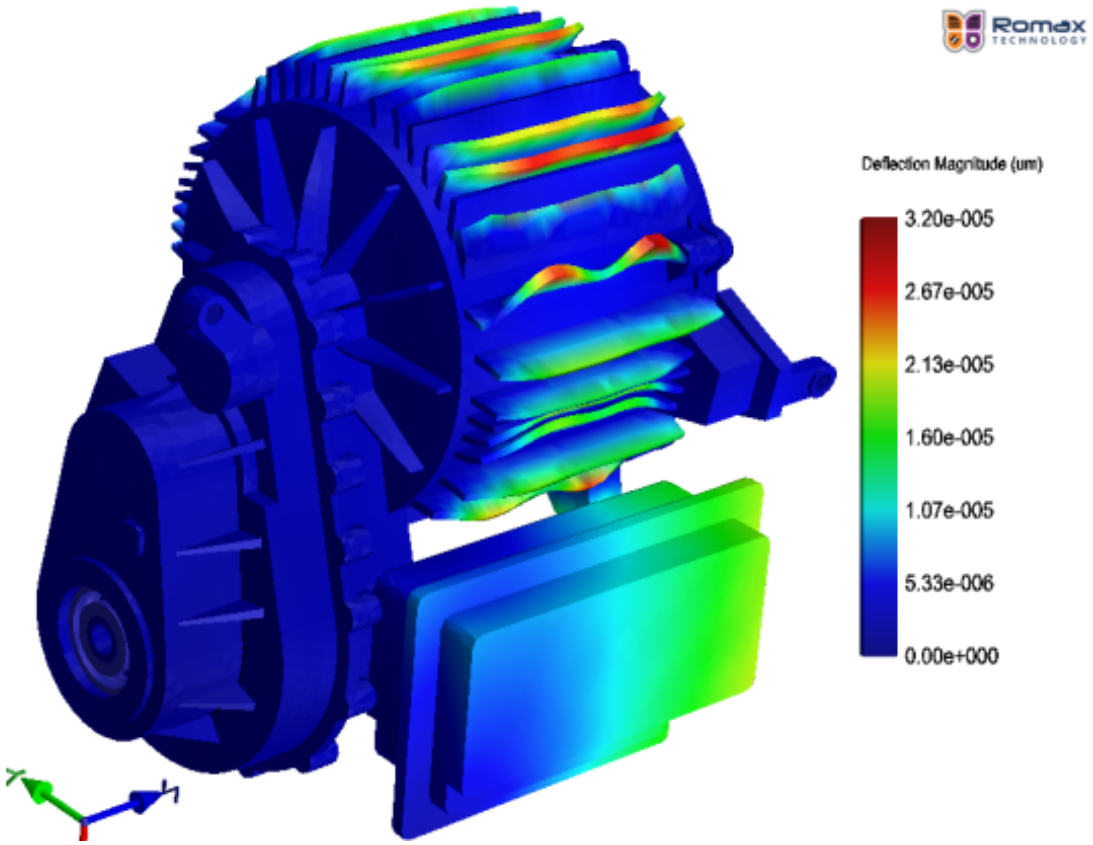

Experimental Evaluation of an Electric Powertrain for NVH

Master's thesis in Applied Mechanics

Praveen Sonnad

DEPARTMENT OF MECHANICS AND MARITIME SCIENCES

CHALMERS UNIVERSITY OF TECHNOLOGY
Gothenburg, Sweden 2023
www.chalmers.se

MASTER'S THESIS IN APPLIED MECHANICS

Experimental Evaluation of an Electric Powertrain for NVH

Praveen Sonnad

CHALMERS
UNIVERSITY OF TECHNOLOGY

Department of Mechanics and Maritime Sciences
Division of Dynamics
Chalmers University of Technology
Gothenburg, Sweden 2023

Experimental Evaluation of an Electric Powertrain for NVH
Praveen Sonnad

Supervisor: Ramkumar Kandasamy, NVH Engineer,Volvo CE
Examiner: Håkan Johansson, Mechanics and Maritime Sciences, Division of Dynamics, Chalmers University of Technology

Master's Thesis 2023
Department of Mechanics and Maritime Sciences
Division of Dynamics
Chalmers University of Technology
SE-412 96 Gothenburg
Telephone +46 31 772 1000

Cover: Example of analysis of an electric powertrain in ROMAX[19]

Typeset in LaTeX
Department of Mechanics and Maritime Sciences
Gothenburg, Sweden 2023

Experimental Evaluation of Electric Powertrain for NVH
Master's Thesis in Applied Mechanics
PRAVEEN SONNAD
Department of Mechanics and Maritime Sciences
Division of Dynamics
Chalmers University of Technology

Abstract

The conventional Internal Combustion (IC) powertrain is now being replaced by alternative, low-emission options, such as the electric powertrain. As a result, the tonal noise and vibration spectrum of the powertrain, previously masked by the IC engine, have become more prominent in the electric powertrain, necessitating an NVH (Noise, Vibration, and Harshness) analysis of the electric powertrain. Previous studies by Vignesh [21] and Anujit [6] utilized a CAE (Computer-Aided Engineering) model to examine the NVH behavior of the electric powertrain under various motor and gearbox excitations, concluding that the highest contribution to the vibration and noise response comes from the motor's torque ripple and the transmission error from the motor. The present study aims to experimentally analyze the NVH behavior of the powertrain and assess the outcome of the earlier study.

The experimental evaluation is being carried out by measuring the vibration, noise, and input shaft speed of the powertrain under different load conditions. The measurement response is then analyzed using the order analysis using fixed sampling method to obtain different acceleration and noise responses of the powertrain with respect to various excitations and their associated orders. The response of the powertrain is studied and compared with the CAE model's behavior.

The comparison between the NVH response of the powertrain obtained from ROMAX model and experimental data yield comparable results. The ROMAX model demonstrated a good correlation with the experimental data for the gearbox excitations. However, for the NVH response from torque ripple, the ROMAX model tended to overestimate the response, even though the peaks in the response align with those in the experimental data. Conversely, the NVH response from the motor's radial and tangential forces were underestimated in the ROMAX model. These observations suggest that the ROMAX model of the powertrain provides a reasonable approximation of NVH response, although fine-tuning the model to better represent the experimental data would yield better results.

Keywords: Electric powertrain, Noise, Vibration, and harshness(NVH), Order Analysis

Preface

This master's thesis, in Applied Mechanics at Chalmers University of Technology, was carried out at Volvo Construction Equipment, Eskilstuna. The thesis work was performed from February 2023 to June 2023 under supervision of Ramkumar Kandasamy at Volvo CE and the examination of Håkan Johansson at the Chalmers University of Technology.

I would like to express my deepest gratitude and appreciation to everyone who has guided and supported me during this thesis.

First and foremost, I would like to thank my supervisor, Ramkumar Kandasamy, NVH engineer at Volvo CE, for his continuous support and guidance during the entire master's thesis project. His expertise in powertrains and mentorship were crucial for the completion of the project.

I would also like to extend my appreciation and gratitude to Magnus Björk, Head of Transmission Development, Volvo CE, for his constant and unwavering support throughout the master's thesis.

I am immensely grateful for the invaluable feedback and guidance provided by Håkan Johansson, professor, Division of Dynamics, throughout the entire course of the master's thesis.

Gothenburg, June 2023

Praveen Sonnad

List of Acronyms

CAE	Computer Aided Engineering
DAQ	Data Acquisition
ERP	Equivalent radiated Power
FFT	Fast Fourier Transform
FRF	Frequency Response Function
GMF	Gear Mesh Frequency
NVH	Noise, Vibration, and Harshness
NPD	New Product Development
ODS	Operating Deflection Shape
PMSM	Permanent magnet Synchronous Motor
RPM	Rotations Per Minute
SPL	Sound Pressure Level
TE	Transmission Error

List of Figures

List of Tables

Contents

1
Introduction

Figure 1.1: EC230 Excavator with an Electric Powertrain

1.1 Background

The world is currently assessing greener alternatives in an effort to reduce dependence on fossil fuels. With that in mind, electric vehicles have emerged as a promising alternative to conventional internal combustion vehicles. Volvo Group, an automotive manufacturer, aims to make 35% of all vehicles sold by the group be electric by 2030 and become fossil-free by 2040 [1]. Volvo Construction Equipment, a subsidiary of Volvo Group and a manufacturer of construction and mining equipment, is leveraging the NPD activities on developing the electric excavator EC230 [2].

Conventional internal combustion (IC) engine vehicles produce a wide range of noise and vibrations originating from the powertrain, with the engine being the primary source of noise. The noise spectrum of the powertrain is typically dominated by the engine order and harmonics in a frequency range below 1 kHz. On the other hand, the electric powertrain produces noise in a higher frequency range from 1 kHz to 10 kHz, which is more noticeable to human hearing and in the absence of an IC

engine, the tonal noise from the electric motor and drive train becomes more noticeable, causing discomfort and annoyance to occupants [4] [9]. Therefore, a noise, vibration, and harshness (NVH) analysis of the powertrain is necessary to identify the source of noise, to reduce and control it.

The noise and vibration sources of the powertrain can be classified into electromagnetic and mechanical sources. Powertrain noise and vibration responses are significantly influenced by motor excitation, electromagnetic sources including cogging torque and torque ripple, as well as mechanical sources such as rotor dynamics, rotor imbalance, bearings, and shaft flexibility. Similarly, the Transmission Error (TE) from the gearbox has a considerable effect on the noise and vibration response of the powertrain.

A CAE model of the powertrain used in EC230 was modeled and analysed by Vignesh [21] and Anujit [6] in 2022. The developed model is based on a few engineering assumptions and correlations. These assumptions are considered to have a negligible impact on the performance of the powertrain. However, to predict the behaviour and study how close the CAE model behaves to reality, an experimental analysis is needed.

1.2 Purpose

The NVH characteristics of an electric powertrain were investigated in the earlier study by Vignesh [21] and Anujit [6]. In order to study the behavior of the powertrain due to electromagnetic and mechanical excitations from the motor and gearbox, they developed a CAE model using tools such as ROMAX [19], ANSYS Maxwell [3]. and MotorCAD [13]. The present thesis aims to repeat the simulations under various load cases, the noise and vibration characteristics of the powertrain are experimentally analyzed, and the CAE model is correlated and compared based on the experimental analysis.

1.3 Limitations

- Excitations from the hydraulic pump were not included in the model, which means that hydraulic pulsation orders are not present in the CAE response.
- The analysis is limited to a permanent magnet synchronous motor and countershaft gearbox powertrain configuration, and the results may not be applicable to other configurations.
- CAE powertrain response of individual excitation types will be evaluated. The response of the system due to a combination of excitations is not evaluated.

2
Theoretical Background

This chapter will introduce and discuss the theoretical background behind the powertrain, electromagnetic-mechanical interaction, and the NVH mechanisms in the electric powertrain.

2.1 Electric Powertrain

The powertrain of the electric excavator EC230 has a Permanent Magnet Synchronous Motor (PMSM), a countershaft axis gearbox, and a hydraulic pump. The powertrain is mounted on four rubber bushes to isolate the powertrain from the excavator chassis.

In Anujit's study [6], an electric powertrain for a heavy machinery application was studied. As mentioned in [10], a system's behaviour can vary drastically from its isolated subcomponents behaviour, but the study of subcomponent behaviour in isolation can provide a good understanding of the overall system. The procedure to study an electro-mechanical system like the powertrain can be subdivided and studied in isolation and then as a whole system, as seen in figure 2.1.

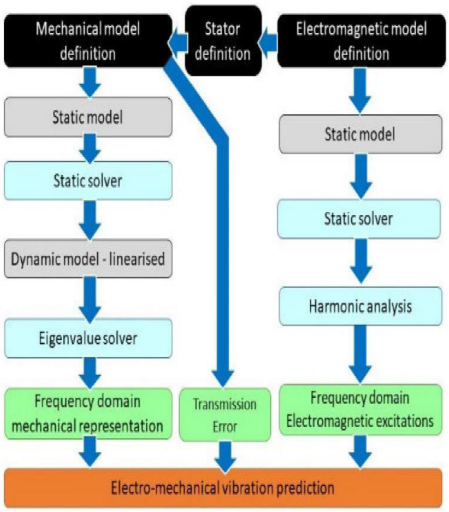

Figure 2.1: Mechanical and electro-mechanical simulation process[10]

It is important to consider the dynamic behavior of individual subsystems, such as the electric motor, gearbox, hydraulic pumps, and auxiliary units individually

since these subsystems can have unique dynamic responses that may differ from their responses when they are integrated into the overall system [7]. Therefore, it is necessary to study the interactions between subsystem excitations and the dynamic response of the system as a whole.

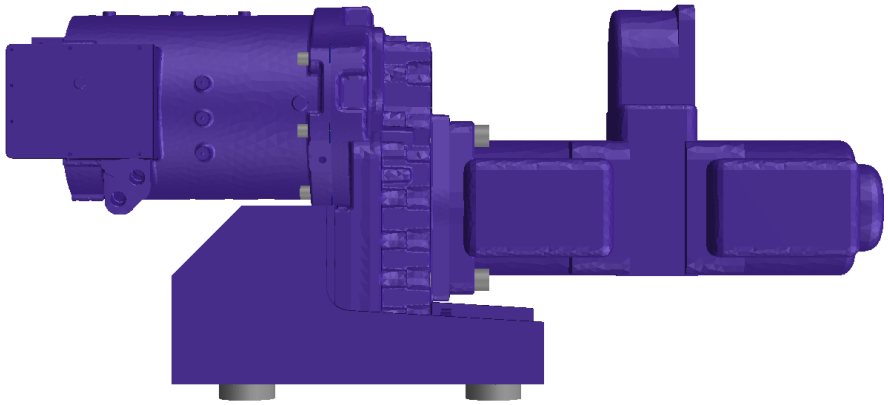

Figure 2.2: Romax model of the powertrain [6]

2.2 Electric Motor

Following the study done by Vignesh [21], the study of the Permanent Magnet Synchronous Motor (PMSM) and previous studies done on the motor are reviewed. In research done by Senousy [14], Dupont [18], Devillers [8], Zhang [22] and Parmar [26] the NVH analysis on electric motor is performed for various excitations. Analysis in the studies includes structural analysis, analysis of radiated noise due to motor defects, and analysis of motor performance under shaft eccentricity. These provide an insight into how the motor can be modelled with various motor excitations in the context of NVH analysis. The simulations are done using ANSYS Maxwell [3], and the dynamic response of the motor under the electromagnetic loads are simulated. These steps are similar in all the mentioned research with varying methodologies focusing on different aspects of motor.

Since the motor excitations from MotorCAD need to be imported into ROMAX, research on similar application by Ha .T [5] on simulations done in ROMAX is studied. This provided a useful insight on how the motor excitations can be obtained and imported into the ROMAX powertrain model

PMSM has been widely used in industries, especially for automotive, construction equipment vehicle, and other high power applications due to its characteristics like high power density and high flexibility for motor construction. PMSM is a hybrid of a brushless DC motor and an induction motor, with field excitations generated from the permanent magnets. Due to its high performance and efficiency and its capability to generate torque at zero speed, it is a suitable choice for automotive applications.

The working principle of the PMSM is similar to that of a three-phase induction motor, where the stator and rotor's rotating magnetic fields interact. However, the PMSM differs in that the rotor consists of a core with permanent magnets embedded in it, and the stator core consists of slots into which the insulated winding is placed. The interaction between the magnetic field of the rotor and the stator's synchronous electric field generates the required rotation of the rotor. In this study, the PMSM has 8 poles and 48 stator slots, as shown in the figure 2.4.

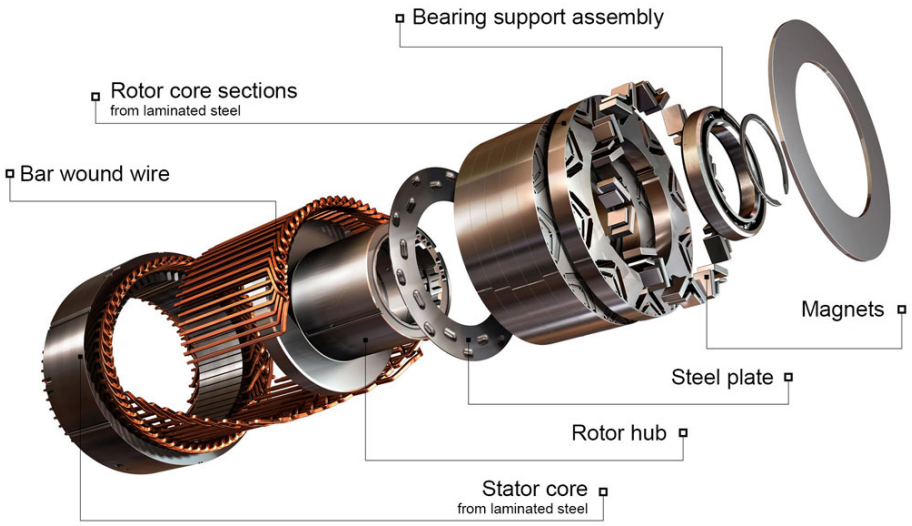

Figure 2.3: Exploded view of a PMSM motor [17]

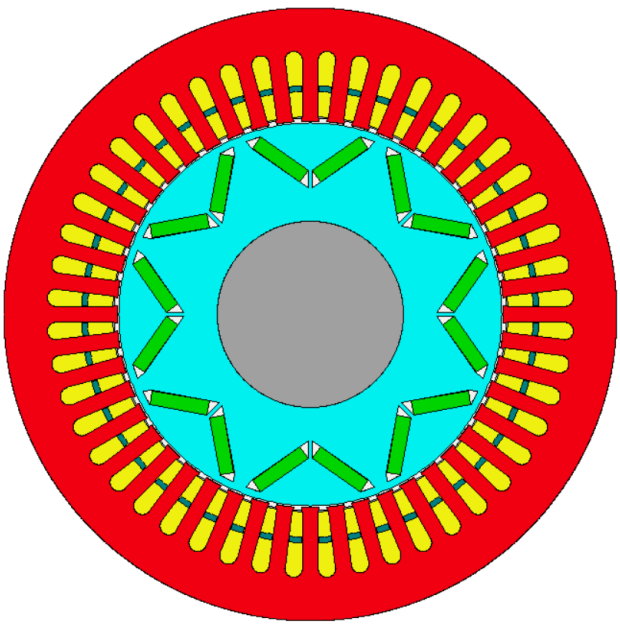

Figure 2.4: Motor model from MotorCAD [13] [21]

2.2.1 Noise and Vibration mechanisms in Motor

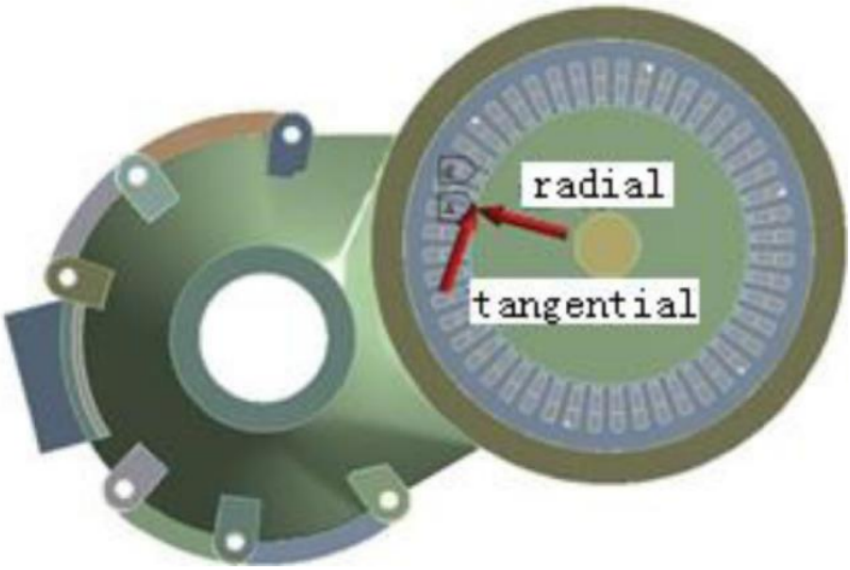

Figure 2.5: Radial and tangential forces in a motor [6]

The noise and vibration generated by a three-phase PMSM can be classified into electromagnetic and mechanical sources. The mechanical sources arise from factors such as bearing defects, shaft imbalance, and surface irregularities resulting from the machining of rotating parts and rotor mounting. On the other hand, electromagnetic sources of noise and vibration are primarily caused by electromagnetic forces and torque ripple that stem from higher harmonics of the supply current, magnetic saturation, phase asymmetry, and disturbances in the magnetic circuit [11].

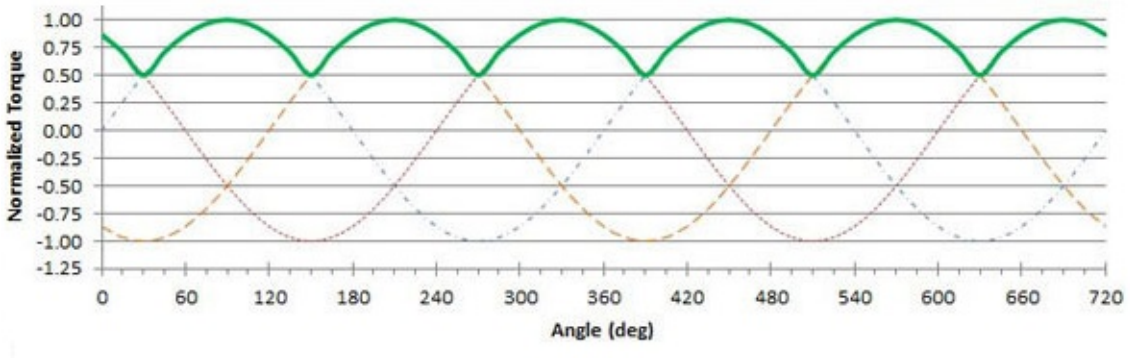

Figure 2.6: Example of Torque Ripple[23]

The Maxwell stress tensor is a mathematical representation of the coupling between electromagnetic forces and mechanical momentum in a system. Specifically, it describes the distribution of forces within the system due to changes in electromagnetic fields. In the case of a PMSM, the Maxwell stress tensor can be used to analyze the

radial and tangential forces generated by the motor [21].

For the purposes of this thesis, the study of motor excitation sources is limited to torque ripple, radial forces, and tangential forces from the motor. Torque ripple refers to the variations in torque that occur as a result of higher harmonics in the supply current, magnetic saturation, and other factors. Radial forces are forces that act perpendicular to the rotational motion, while tangential forces act parallel to the rotational motion. The electromagnetic forces and torque ripple generate vibrations that propagate through the stator and rotor to the housing, resulting in structure-borne noise. The radial and tangential forces, on the other hand, cause the rotor to deviate from its intended axis of rotation, resulting in imbalance and air-gap eccentricity. This in turn generates additional vibrations and noise.

2.3 Gearbox

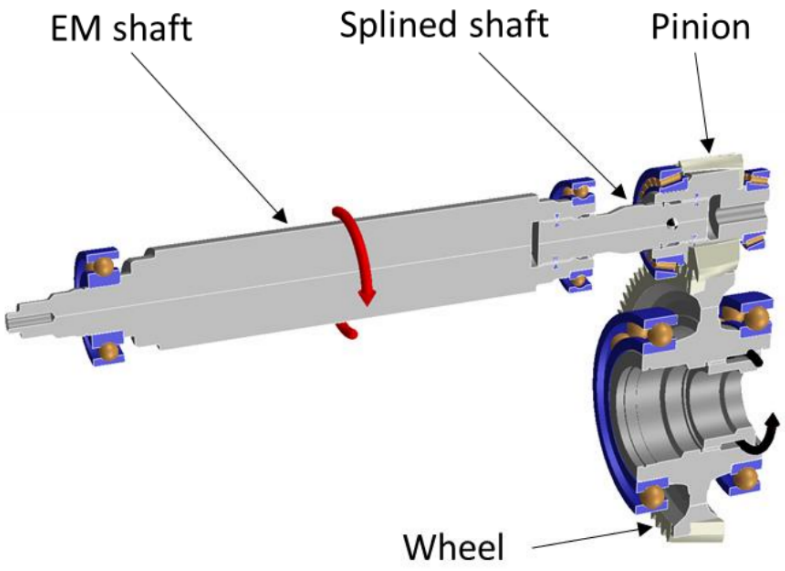

Figure 2.7: Helical gearset connected to motor input shaft [6]

The transmission box, also known as the gearbox is the second element of the power train in a construction equipment vehicle. It is used to change the speed and torque of a vehicle according to a variety of road and load conditions. Volvo CE uses countershaft axis gearbox in the EC230. The countershaft axis gearbox is responsible for transmitting the torque from the PMSM to the hydraulic pump. The gearbox consists of a single helical gearset that transfers the power from the motor to the hydraulic pump. The helical gearset is preferred over other types of gearsets due to its ability to reduce noise and vibration generated during gear engagement. The gearset is enclosed within a housing that is filled with lubricating oil to reduce

wear and tear, as well as dissipate heat generated during the gear operation. The mechanical excitation sources of the gearbox can be attributed to gear meshing, bearing rotation, shaft bending, and gearbox housing deformation. The vibration and noise generated by the gearbox are mainly due to the excitation sources and their interaction with the surrounding structure, such as the rubber mounts and the excavator chassis. Therefore, the gearbox's NVH analysis is crucial to evaluate the system's overall noise and vibration performance.

2.3.1 Noise and Vibration mechanisms in Gearbox

The largest contributors to noise and vibration in the gearbox is Transmission Error (TE), although it is not the only source [12]. TE can be defined as "the difference between the actual position of the output gear and the position it would occupy if the gear drive were perfectly conjugate." The causes of TE include flexibility of the gear tooth, gear blank, bearing, housing, and shaft, which results in variations in force and contact in the gear mesh.

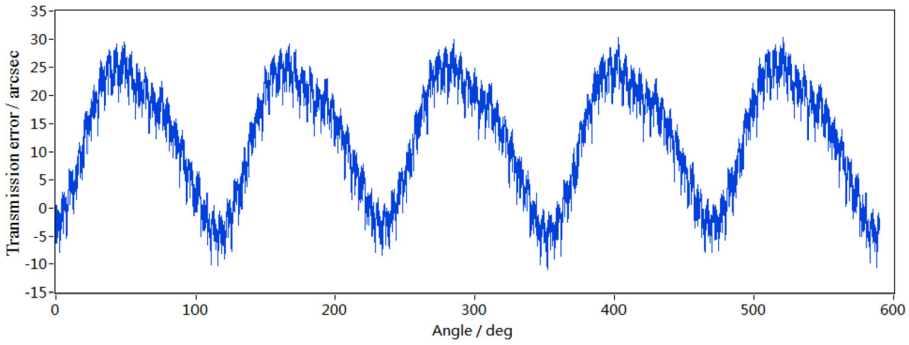

Figure 2.8: Transmission Error(TE) example [29]

In addition to TE, the gear tooth mesh is another critical source of vibration in gearboxes. The meshing of gear teeth can excite resonances in other components, such as the bearings, housings, and shafts, which can lead to noise and vibration. The natural frequencies of these components, their damping characteristics, and the input excitations are all important factors to consider when predicting the dynamic behavior of the gearbox. Accurately predicting the dynamic behavior of the gearbox is crucial for designing effective noise and vibration reduction strategies.

2.4 Experimental Analysis

A comprehensive study to review the existing research, methodologies, and analysis techniques for electric powertrains, in context of NVH, were examined. The study involved exploring experimental measurement techniques, measurement and analysis techniques, and data analysis for NVH analysis of an electric powertrain.

To review experimental measurement techniques, the required sensors and measurement setup, study by Panza [15] were examined to appropriately capture the noise

and vibration response of the system. This paper by Panza [15] talks about common measurement techniques like measuring sound pressure level (SPL), commonly used accelerometers and microphones, and data acquisition systems were examined for NVH application.

Signal analysis and interpretation of experimental data require investigating statistical analysis techniques, data processing methods, and data visualisation. To extract meaningful data from the raw NVH measurement data, techniques like spectral analysis, order tracking, and modal analysis were explored [25], [16]. The study by Petrovsky [16] and Anders Brandt [25] discuss order analysis, methods, and drawbacks of order analysis methods. Order analysis with uniform sampling method. This method is faster, but the processed signal has a lot of smearing. Conversely, the order tracking method is more accurate but computationally expensive. Reviewing [27] illustrates the fundamentals of signal processing and the different methods involved. Spectral leakage during signal processing can be drastically reduced by using proper windowing techniques as discussed by Anders Brandt [25].

2.4.1 Order Analysis

Waterfall analysis is a powerful tool for identifying the resonance frequencies and orders of the system, as it can be used to analyze the vibration or noise signals together with the motor speed signals. This approach can provide an understanding of how the different components of the system are interacting with each other and how they are contributing to the overall vibration and noise levels.

The order analysis is typically performed using a waterfall plot, figure 2.9, which is a graphical representation of the frequency content of a signal as a function of speed and frequency. The x-axis of the plot represents frequency, the y-axis represents shaft speed, and the color or intensity of the plot represents the magnitude of the corresponding frequency component. Waterfall analysis is done by performing FFT on the measured time series data at uniform time intervals and the FFT data are then stacked up. The vertical lines in the waterfall plot represent the resonance at different frequencies, and the diagonal lines represent the harmonic orders with respect to the shaft speed. The speed of different components like gears and pumps in the powertrain are dependent on the motor speed, and component speed varies with the motor speed. The response of the components are represented as its harmonic orders as diagonal lines, varying with respect to motor speed.

2.5 Sound pressure Level (SPL)

Sound pressure level (SPL) is a logarithmic measure of sound pressure radiated from a surface relative to a reference value. It is a measure of the intensity of sound at a particular point. SPL (dB) is defined as the ratio of sound pressure P to reference sound pressure P_0 (20 µPa for airborne sound). SPL is used to assess the potential

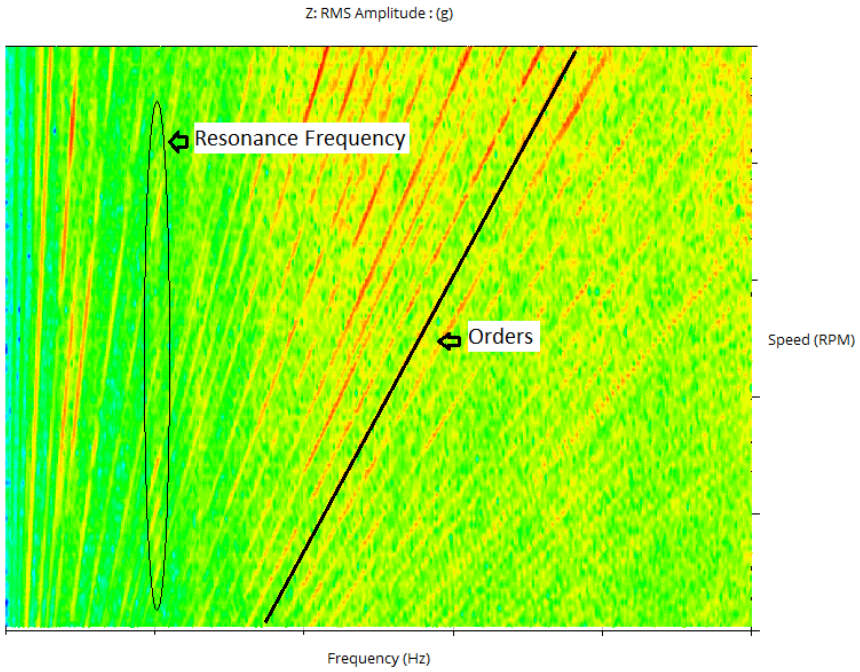

Figure 2.9: Waterfall plot

for hearing damage and evaluate the sound dampening required and its effectiveness.

$$SPL = 20 * log_{10}(\frac{P}{P_0})$$

3
Method and Implementation

3.1 The Powertrain Studied

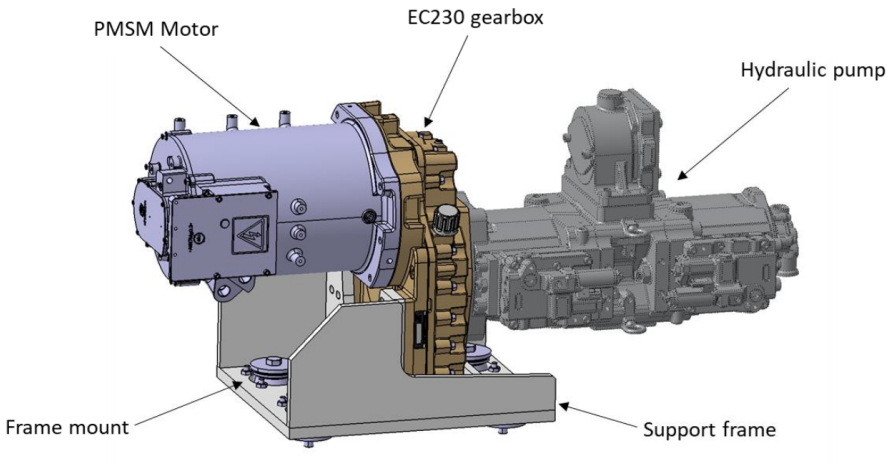

Figure 3.1: EC230 Powertrain CAD model[6]

The powertrain studied in this thesis is a countershaft gearbox used in the EC230 excavator from Volvo Construction Equipment, Volvo Group. See figure 3.1 for the CAD model of the powertrain. It is used to power the hydraulic systems of the excavator, the powertrain consists of an PMSM electric motor, a single-stage reduction gearbox, and a hydraulic pump. The gearbox, with a fixed reduction of 2.81, has a single helical gearset connecting the input and output shafts. The input shaft is supported by two SKF tapered roller bearings, and the output shaft is supported by two SKF deep groove ball bearings. A splined intermediate shaft connects the motor and the input shaft of the gearbox, and another splined shaft similarly connects the hydraulic pump with the gearbox.

The helical gearset in the gearbox has a gear ratio of 2.81. The pinion gear has 27 teeth, and the driven gear has 76 teeth. The PMSM has a 3-phase, 8-pole, 48 stator teeth electric motor. The motor, gearbox, and hydraulic pump are bolted onto the support frame, and the assembly is mounted on the excavator chassis using rubber mounts to isolate the system from the chassis.

3.2 CAE Modelling

The CAE model is built using ROMAX, the motor shaft, gears, gearblanks, and connections are modeled in ROMAX with the motor, gearbox, and pump housing FE imported into the model. Motor excitation forces are extracted from MotorCAD and imported into ROMAX. Motor-CAD provides three modules, EMag + Therm + Lab, that enable very fast calculations of motor efficiency maps and subsequent thermal transient analysis of different complex duty cycles/drive cycles.

3.2.1 Motor excitation forces from MotorCAD

MotorCAD is a software tool used for the electromagnetic and thermal analysis of electric motors. It includes various tools for the design and optimization of electric motors, such as electromagnetic analysis, FE analysis, thermal analysis, and design optimization tools. The excitation forces for required load cases, such as radial and tangential forces and torque ripple, are determined using MotorCAD, following the method and procedure mentioned by Vignesh [21].

The software has pre-defined templates for different types of motors. A motor model can be quickly created by providing the motor parameters like stator diameter, stator bore diameter, number of slots and slot dimensions, number of poles in the rotor, permanent magnet dimensions, etc. into these templates. The parameters of the electric motor are as obtained from Vignesh [21]. The motor model can then be analysis in different environments such as E-Magnetic, Thermal, Lab, and Mechanical.

3.2.1.1 E-magnetic

E-magnetic module performs FE analysis on the motor model. The module calculates the back emf, cogging torque, and magnetic flux density plots of the motor. The analysis process begins with defining the geometry, material properties of the stator, rotor, winding and permanent magnets in MotorCAD material database as per [21]. The winding definition is defined as per table 3.1 in the next step.

Property	Value
Winding type	Lap
Path type	Upper-Lower
Coil	Stranded
Wire Size	XXX-XXX mm

Table 3.1: Winding specification [21]

The operational losses in the motor need to be updated into the model in MotorCAD. Losses are categorised into three types, iron loss, bearing loss, and AC winding loss. Iron losses or core losses are caused by eddy currents and hysteresis in the core, and are calculated in MotorCAD using Steinmetz's equation. Bearing losses are input

directly from experimental values obtained from Volvo CE. AC winding losses are calculated by hybrid FEA [21].

After the components are meshed as per table 3.2 and input parameters for the motor such as shaft speed, peak current, and motor component temperatures are defined as per [21], the model definition is completed. The E-magnetic module is solved to get the electromagnetic behaviour of the motor.

Part	Mesh size
Stator	1 mm
Rotor	1 mm
Airgap layers	4
Airgap surface points	720
Airgap internal points	720

Table 3.2: Mesh size for MotorCAD [21]

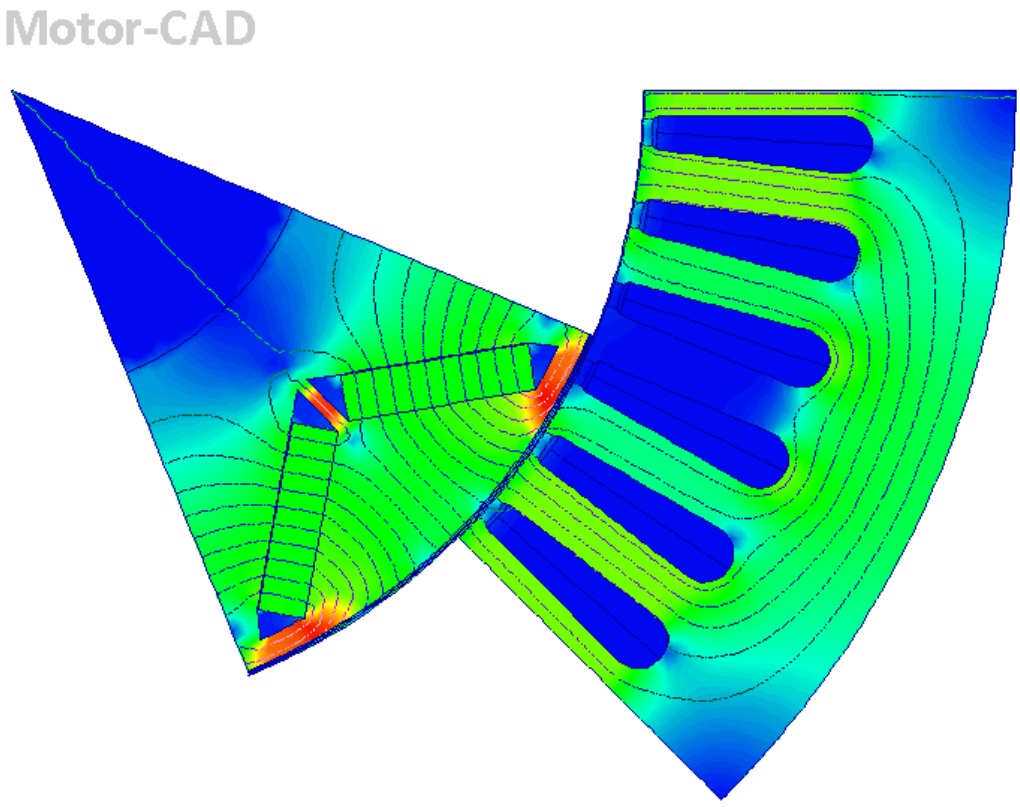

Figure 3.2: Magnetic flux density at 2000 RPM and 220 Nm torque

3.2.1.2 Lab

Lab Module calculates the efficiency maps and torque-speed curves of the motor.

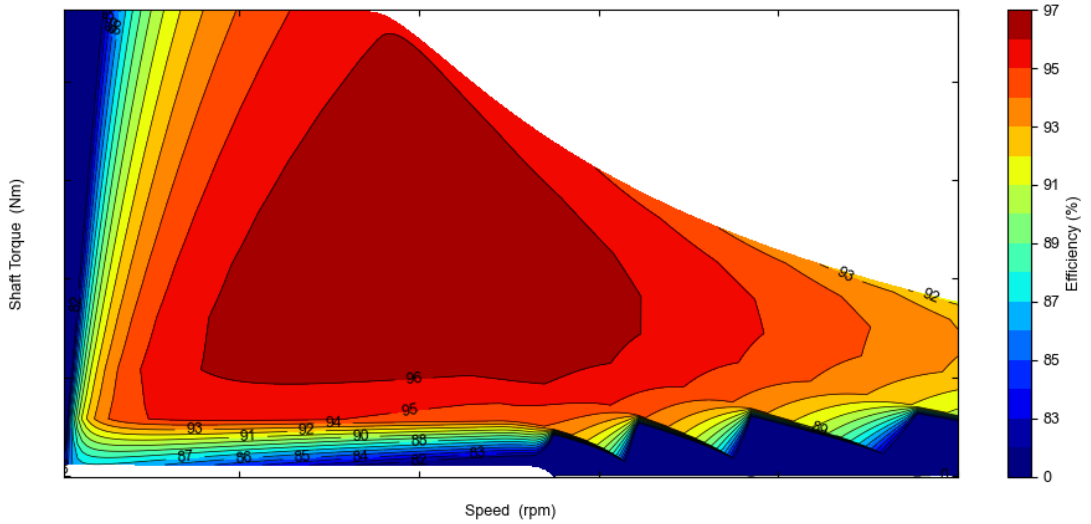

Figure 3.3: Efficiency map of the motor

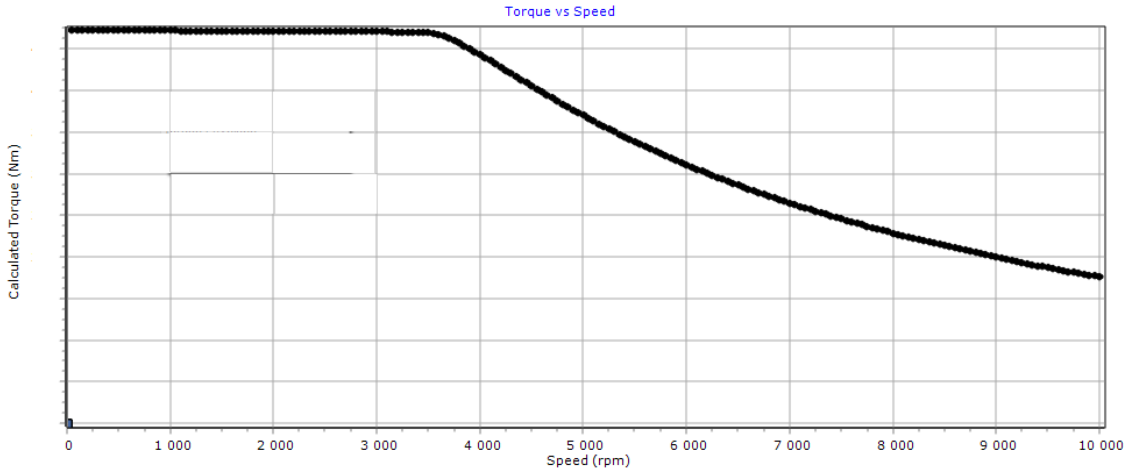

Figure 3.4: Torque envelope of the motor

3.2.1.3 Mechanical

The torque and speed points required for ROMAX are updated in the mechanical module, and simulation is run to obtain the motor excitation forces. The requested load points on MotorCAD are as mentioned in table 3.3.

Requested Torque (Nm)	Speed (RPM)
220	1000
220	2000
220	3000
220	4000
220	5000
110	1000
110	2000
110	3000
110	4000
110	5000
55	1000
55	2000
55	3000
55	4000
55	5000

Table 3.3: Torque points in MotorCAD

3.2.2 ROMAX model

ROMAX is a widely used software in the automotive industry for the design and analysis of powertrains. ROMAX DT is a module used specifically for powertrain NVH analysis. Various types of NVH analyses can be performed using ROMAX DT, including modal analysis, frequency response analysis, time domain analysis, and multi-body dynamics simulation. These analyses help identify and address various NVH issues, such as gear whine, bearing noise, transmission rattle, and gear tooth impact.

To perform noise and vibration simulations in ROMAX, the motor excitation from MotorCAD is imported into ROMAX following the method and procedure described by Anujit [6].

3.2.2.1 Shafts

The key components of the powertrain, which include the motor shaft, gears, and splined shafts, are modeled in ROMAX. These components are assembled onto appropriate bearings, and splined connections between shafts are modeled as rigid connections (RBE2) as illustrated in figure 3.5. Gear blanks are integrated into the shafts and are modeled similar to a shaft, ROMAX facilitates easy modeling of gearsets by defining the gear geometry and selecting the shafts to mount the gears on, as illustrated in figure 3.6 and 2.7.

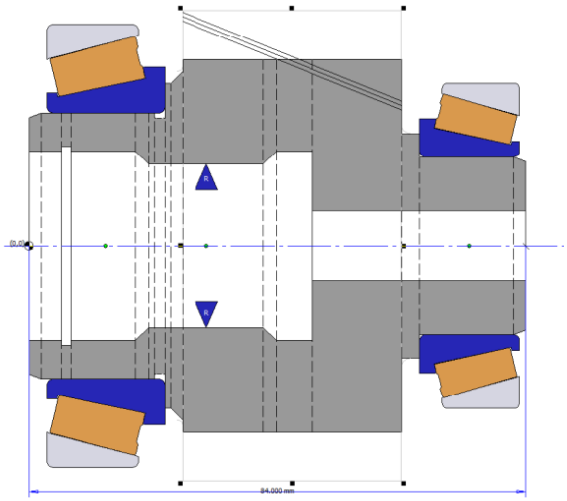

Figure 3.5: Shaft model in ROMAX with bearings and rigid connections[6]

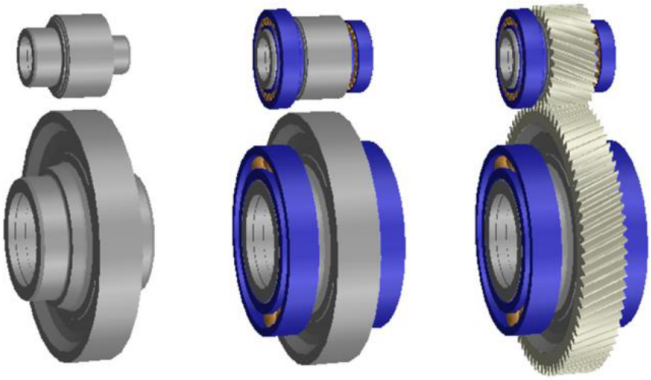

Figure 3.6: Gearset model in ROMAX[6]

3.2.2.2 FE model of motor, gearbox and pump housing

The motor, gearbox, and pump housing CAD model is imported and meshed in ANSYS workbench [3] after defeaturing in SpaceClaim [3] as illustrated in figure 3.7. The FE models are imported into ROMAX and positioned using the bearings and other connections mentioned in 3.2.2.1 using rigid connections (RBE2) as illustrated in figure 3.8 with mesh details of the components in table 3.4.

Component	Element Type	No. of elements	Material
Gearbox	Second order tetrahedral	420,908	Isotropic
Hydraulic Pump	Second order tetrahedral	280,398	Isotropic
Electric Motor	Second order tetrahedral	252,621	Isotropic

Table 3.4: FE Model Mesh size for ROMAX [6]

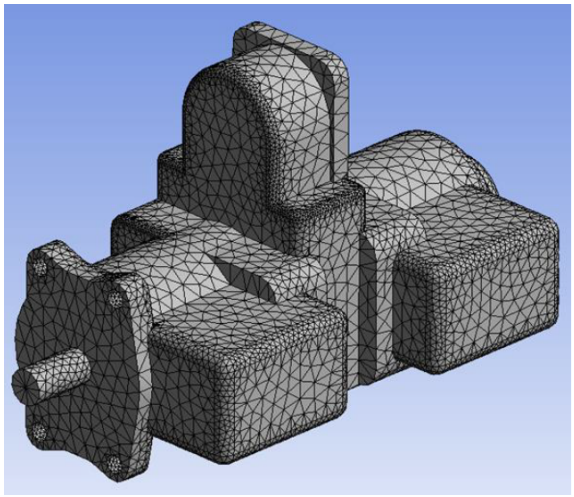

(a) Hydraulic Pump housing FE model

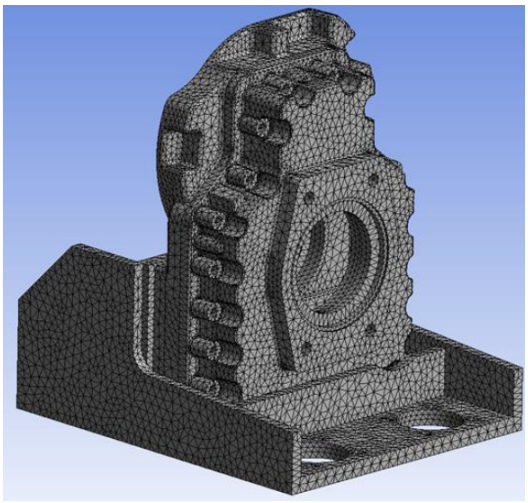

(b) Gearbox housing FE model

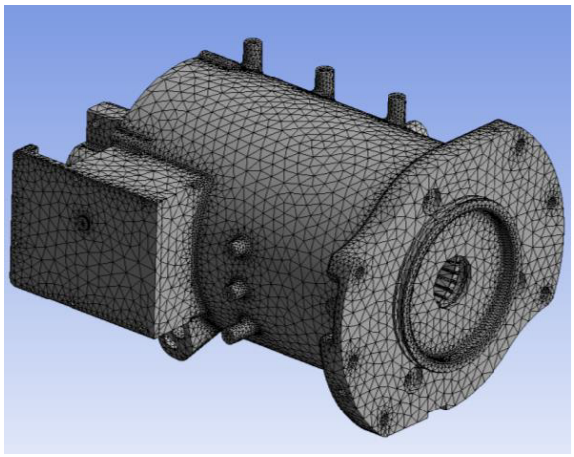

(c) Motor housing FE model

Figure 3.7: Meshed FE model in ANSYS [3] [6]

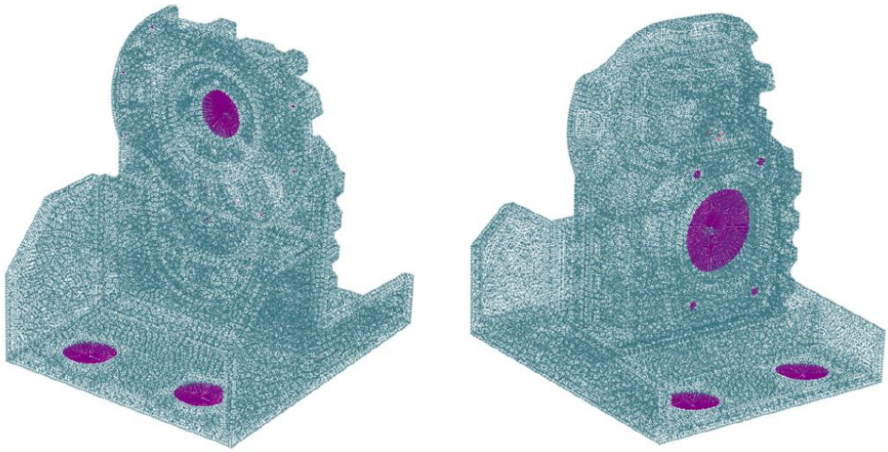

Figure 3.8: Positioning the Gearbox FE model in ROMAX[6]

3.2.2.3 Motor excitations from MotorCAD in ROMAX

The electric motor is modeled by defining the number of phases, pole pairs, stator slots, etc from [21]. Excitation forces from MotorCAD are imported into ROMAX and motor harmonics are calculated as seen in figure 3.9.

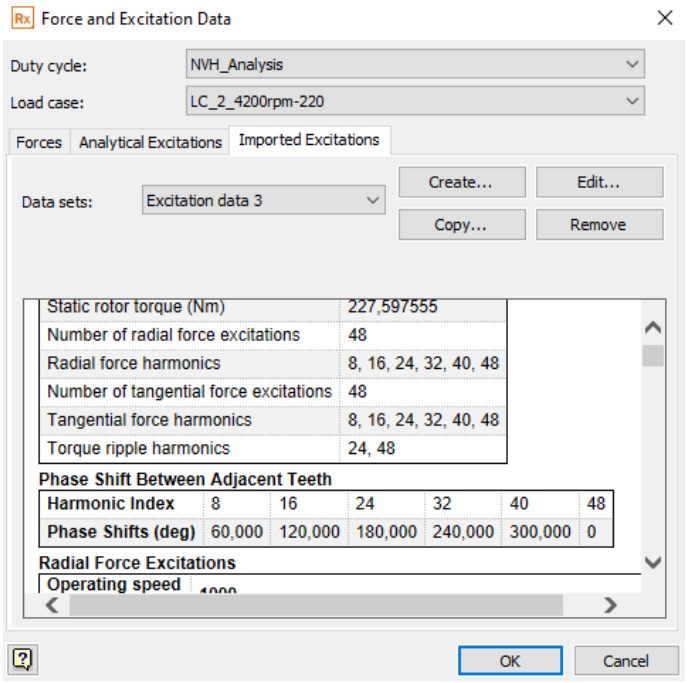

Figure 3.9: Motor Excitation data for 100% loadcase

3.2.3 Boundary conditions and Loadcases

3.2.3.1 Boundary Conditions

The powertrain assembly is mounted on the excavator chassis using rubber mounts to isolate the excavator chassis from the powertrain. This is replicated in the model, where the powertrain is constrained to the ground with a rigid connection with rubber mounts. The rubber mount stiffness is obtained from [6].

3.2.3.2 Loadcases

The simulation is performed for various loadcases as defined in 3.5. The loadcases are selected to replicate the torque required for the hydraulic pump at different loads.

LC	Torque	MotorCAD excitation speeds	Motor speed
1	220 Nm	1000, 2000, 3000, 4000, 5000 RPM	0-5000 RPM
2	110 Nm	1000, 2000, 3000, 4000, 5000 RPM	0-5000 RPM
3	55 Nm	1000, 2000, 3000, 4000, 5000 RPM	0-5000 RPM
4	17.5Nm	1000, 2000, 3000, 4000, 5000 RPM	0-5000 RPM

Table 3.5: Powertrain Load cases

3.2.4 NVH Simulation

After the powertrain model is complete and the excitation forces from the motor are imported into the model, displacement in gear tooth along the line of action and average tooth mesh stiffness are calculated. The average tooth mesh stiffness and displacement gives the TE force excitations over a single tooth. TE forces are then used for the vibration and acoustic analysis. The excitation forces from TE, motor radial and tangential forces, and torque ripple are now used for the NVH analysis of the powertrain. The vibration response of the system at different response nodes can now be obtained through the vibration analysis module, as depicted in figure 3.10. Similarly, the acoustic response of the system can be obtained from the acoustic analysis module, see figure 3.11. The acoustic analysis should ideally be performed with a shrinkwrap on the whole powertrain, as seen in figure 3.12, due to limited computational capacity, the acoustic shrinkwrap was done on individual sub-components, as seen in figure 3.12. The acoustic results represent the radiated noise from each subcomponent's shrinkwrapped body under both motor and gearbox excitation.

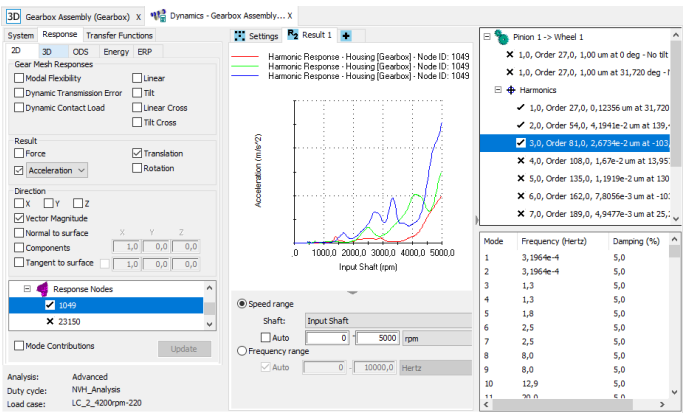

Figure 3.10: Vibration analysis for 100% loadcase using ROMAX

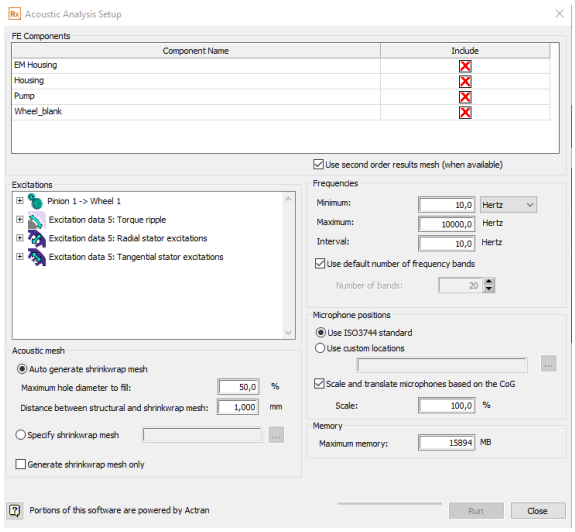

Figure 3.11: Acoustic analysis in ROMAX

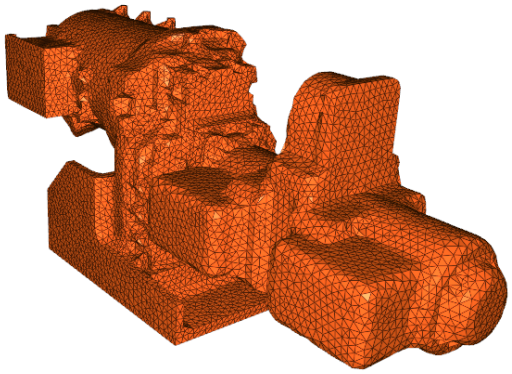

Figure 3.12: Acoustic shrink wrap of the powertrain

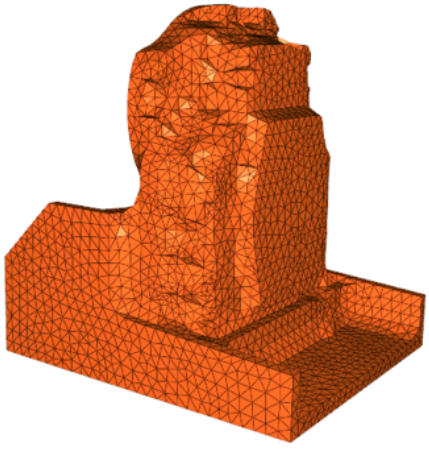

Figure 3.13: Acoustic shrink wrap for Gearbox

3.3 Measurement

3.3.1 Test Set-up

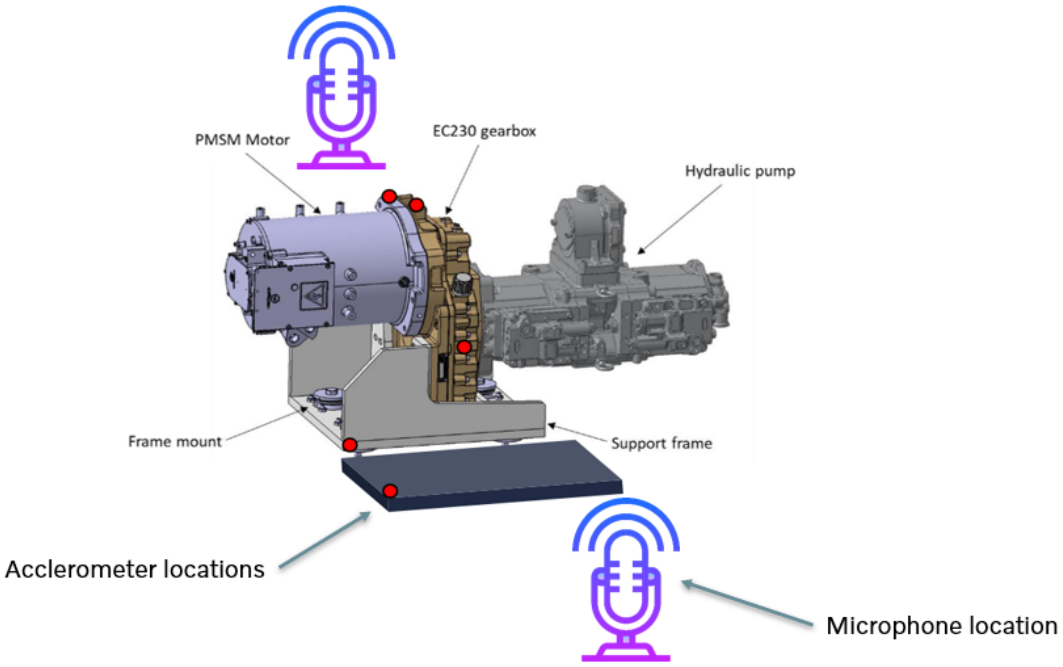

Figure 3.14: Accelerometer and microphone location

System analysis often involves measuring different parameters to understand the dynamic behavior and noise response of the system. In the case of NVH response of a system, acceleration response and sound pressure levels are two key parameters required to study the dynamic and noise response of the system.

To measure the acceleration response, sensors are placed at multiple locations, such as the top and side of the gearbox, the mounting flange of the electric motor, and before and after the rubber mounts. These locations are chosen based on their potential impact on the vibration characteristics of the system. By measuring the acceleration response at these locations, it is possible to validate the system model and identify any potential issues such as resonance or excessive vibration levels.

Similarly, to measure the sound pressure levels, two microphones are placed on the left and right sides of the gearbox at a distance of 1 m. This allows for the measurement of noise emissions from the gearbox and can help identify potential noise sources. The information obtained from these measurements can be used to develop noise reduction strategies and improve the overall performance of the system. The motor speed and torque are measured and obtained from the vehicle's Controller Area Network (CAN). CAN is a message-based protocol that enables high-speed communication and real-time control of various vehicle systems, including the engine, transmission, and braking systems. Figure 3.19 depicts the placement of the

accelerometer and microphone on the testrig.

3.3.2 Test Equipment

3.3.2.1 Sensors

Accelerometers

Figure 3.15: Accelerometer

The PCB Piezotronics accelerometer model HT356B21 is a high-temperature, quartz shear sensing device designed for measuring vibrations and shock in harsh environments. It can measure accelerations up to ±500g with a sensitivity of 5mV/g. The HT356B21 accelerometer is designed with a robust, hermetically sealed, stainless steel housing that can withstand high temperatures and harsh environments. It also features a top connector for easy installation and maintenance, making it ideal for powertrain and NVH application [24].

Precision microphones

Figure 3.16: Precision Microphone

The PCB Piezotronics condenser microphone model 377A20 is a precision microphone designed for measuring acoustic pressure fluctuations. It has a nominal diameter of 1/2 inch and a frequency response range of 4 to 25,000 Hz, with a lower limiting frequency of 1 to 2.4 Hz. The microphone has an open circuit sensitivity of 12.6 mV/Pa at 250 Hz and a dynamic range of 162 dB with a 3% distortion limit. It operates in a temperature range of -40 to +248 °F (-40 to +120 °C) and has a stainless alloy housing material with rear venting. The microphone has a polarization voltage of 0 V and a capacitance of 14 pF.

The microphone model 377A20 requires a preamplifier to function properly. The Model 426E01 preamplifier from PCB Piezotronics is used for measurements as it is designed specifically for use with condenser microphones and can provide a voltage output for the microphone signal. The 426E01 preamplifier has a high input impedance to prevent loading of the microphone and can operate on a variety of power sources, including batteries, AC power, or DC power. The preamplifier also includes a low-pass filter to help reduce unwanted noise and can be mounted directly to the microphone for convenience.

3.3.2.2 DAQ system

Figure 3.17: Data acquisition module

The Simcenter SCADAS Mobile 05 is a portable measurement system designed for acquiring and analyzing dynamic signals in various testing environments. The system features up to 16 simultaneously sampled channels, with a dynamic range of 24 bits and a maximum sample rate of 204.8 kS/s per channel. The device is capable of acquiring signals from a wide range of transducers, including accelerometers, microphones, strain gauges, and thermocouples.

3.3.2.3 Software

Simcenter Testlab [20] is a comprehensive platform for test-based engineering to perform a wide range of tests, including acoustics, vibration, durability, and structural analysis. Simcenter Testlab serves as the primary software platform for data acquisition, processing, and analysis.

Simcenter Testlab provides a user-friendly interface that allows users to set up and configure data acquisition channels, manage measurement files, and perform signal processing and analysis tasks. With its advanced post-processing capabilities, Simcenter Testlab can perform complex data analysis tasks such as frequency response function (FRF) analysis, modal analysis, and sound quality analysis.

3.3.3 Procedure

LC	Hydraulic load	Motor Load	Motor Torque	Motor speed
1	100%	50%	220 Nm	2000-4500 RPM
2	50%	25%	110 Nm	2000-4500 RPM
3	25%	12.5%	55 Nm	2000-4500 RPM
4	0%	4%	17.6 Nm	0-4500 RPM

Table 3.6: Powertrain Load cases for Testing

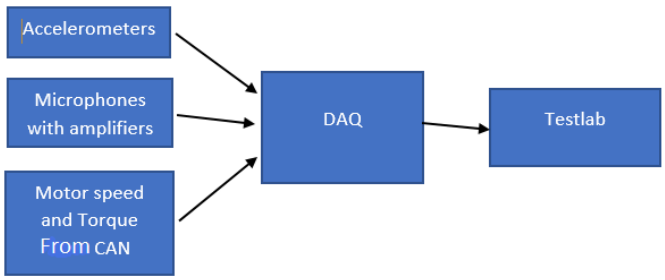

Figure 3.18: Test equipment connection schamatic

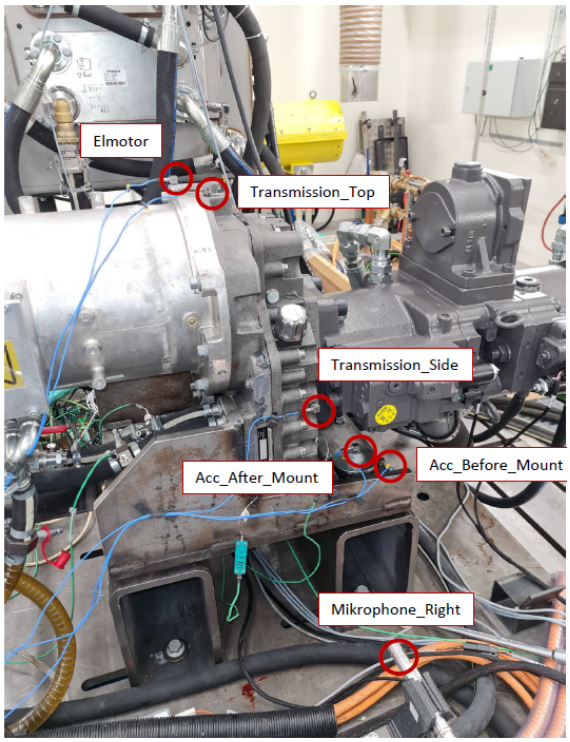

Figure 3.19: Experimental Setup

The test equipment is connected and set up as seen in figure 3.18 and figure 3.19. Experimental analysis on the powertrain is done using nCode[28] using the VibeSys module. VibeSys is a module in nCode. The VibeSys module is specifically designed for structural dynamics and vibration analysis of complex mechanical systems. It is used to predict and evaluate the vibration behavior of structures, components, and assemblies due to dynamic loads.

A total of nineteen test signals were recorded for the powertrain runup. This includes the motor speed, motor torque, left and right measured sound pressure levels, X-Y-Z axis accelerations for the electric motor, gearbox top and side, before and after rubber mount location on the powertrain, figure 3.20 illustrates the two noise and two vibration signals measured for three load cases. Load cases 25% 50% and 100% are recorded in the same signal for a total duration of 900 seconds. Runup is performed by linearly increasing the motor speed from 2000 RPM to 4500 RPM, as seen in figure 3.21. The measured noise response is in Pa, and the measured acceleration response is in standard gravity g.

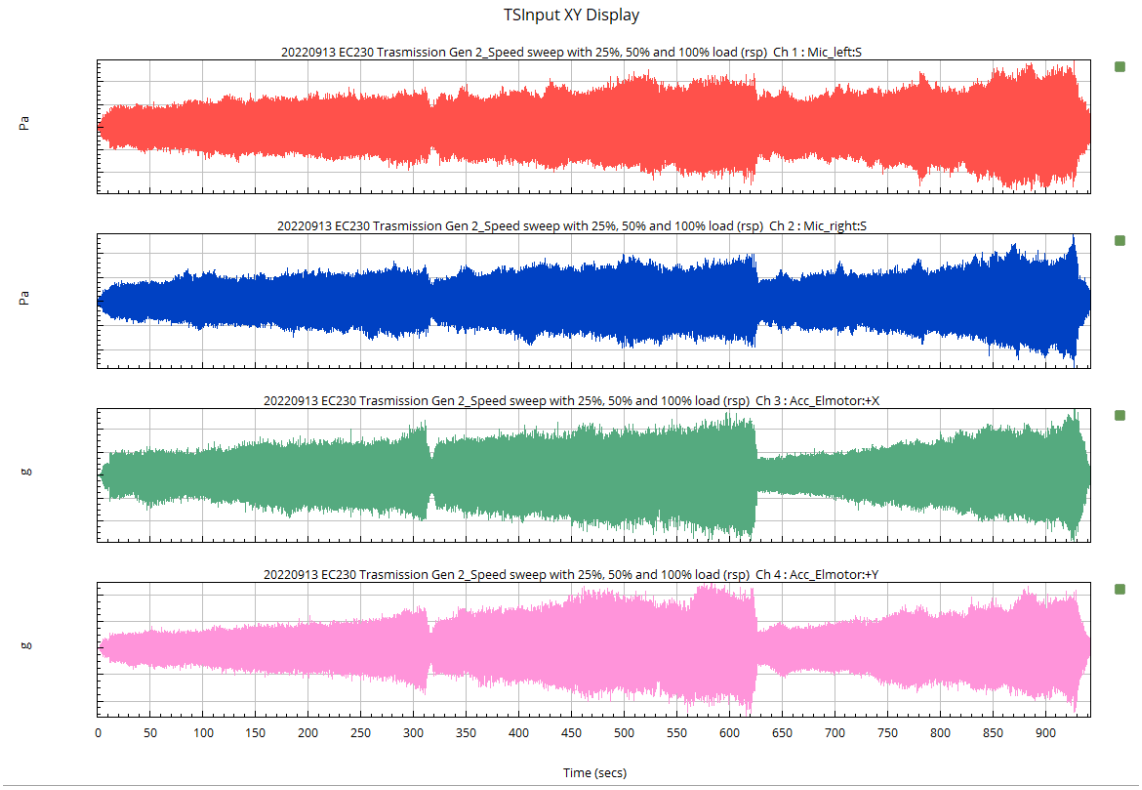

Figure 3.20: Recorded signals

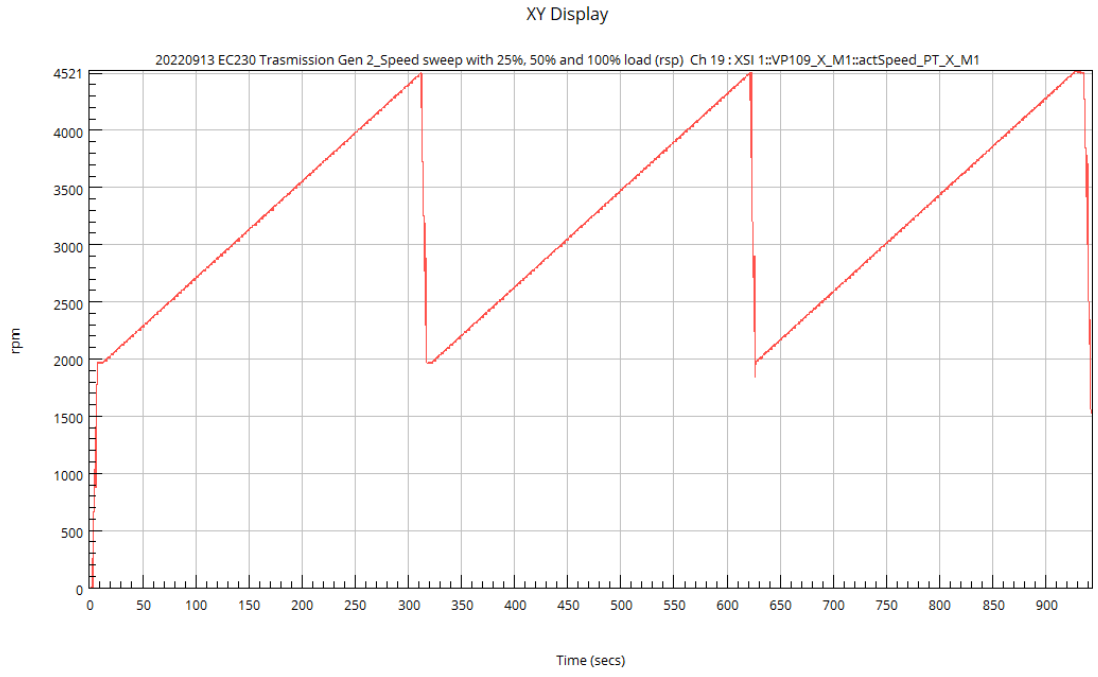

Figure 3.21: Recorded Speed signal

Figure 3.23 provides an overview of the signal analysis process. The process starts with the extraction of signals for each load case, which are then processed using the

waterfall analysis glyph. The waterfall analysis technique involves performing FFT analysis at different speeds, and these FFTs are then stacked. The stacked FFT's can be visualised as a waterfall plot in figure 3.22.

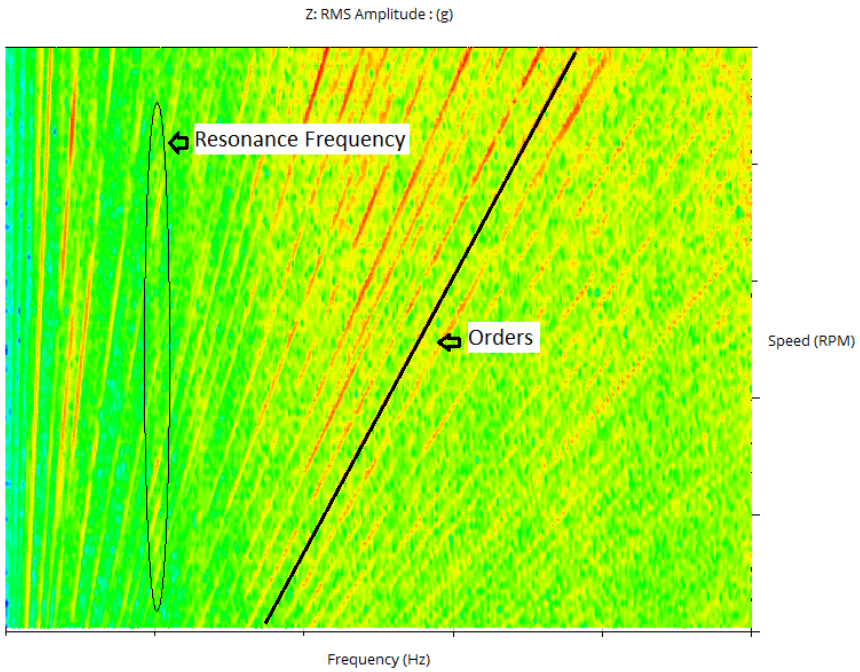

Figure 3.22: Color map illustrating waterfall plot for acceleration

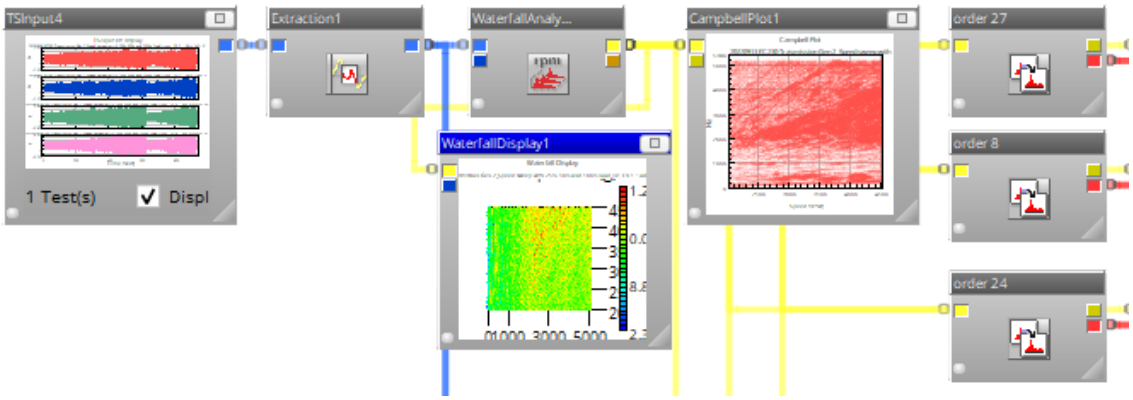

Figure 3.23: Signal analysis workflow

For this powertrain application, the hanning window method [25] is employed with an appropriate buffer size to ensure that the frequency response of the system is accurately captured. The complex frequency manipulation glyph slices the waterfall data to produce the frequency response at specific orders.

Order tracking or order based resampling is a more accurate method of obtaining system response at each order, but it is computationally expensive. The slicing

method using complex frequency manipulation can be equally accurate when used with an appropriate order bandwidth.

3.4 Comparison Between CAE and test data

The comparison of noise and acceleration response data from both CAE and experimental sources needs to be accurately compared. To facilitate this comparison, the acceleration and noise response data for each order is exported into a .csv file and subsequently processed using Python.

It is important to note that the noise and acceleration response data from CAE is typically reported in SPL(dB) and m/s^2, respectively. Therefore, in order to properly compare this data to the experimental results, the noise response data from the experiment must first be converted into SPL (dB) using an appropriate formula. Likewise, the acceleration response data from the experiment must be converted into m/s^2 by multiplying the values by the gravitational constant g, which has a value of approximately 9.81 m/s^2. By converting the noise and acceleration response data from the experimental source to the same units as the CAE data, the resulting datasets can be properly compared and analyzed.

4
Results and Discussion

Harmonics	Hydraulic	Gearbox	Motor
1	3.2	27	8
2	6.4	54	24
3	9.6	81	32
4	12.8		48

Table 4.1: Powertrain orders of interest

The section describes and analyses the results for the 100% load case, results for 50% and 25% loadcase are in the appendix. The prominent harmonic orders of the powertrain can be categorized into hydraulic, gearbox, and motor excitations. The hydraulic pulsation has orders 9, 18, 27, 36, etc. with respect to the pump input shaft, which, when multiplied with the gearbox ratio, become orders 3.2, 6.4, 9.6, 12.8, etc. with respect to the motor speed, with the highest response at order 51.2. The pinion gear is connected to the motor output shaft and has 27 teeth, thus having orders 27, 54, and 81. Radial and tangential forces influence orders 8, 24, and 32, and torque ripple influences orders 24 and 48.

4.1 Load Case 1 100% load

4.1.1 Noise

4.1.1.1 Gearbox Excitation Orders

The comparison between CAE data and test data for gearbox excitation orders 27 and 54 provides a valuable insight into the noise response of the powertrain due to the gearbox excitation. Figures 4.1 and Figure 4.2 demonstrate that the speeds at which the peaks occur in CAE data closely align with measurement data speeds. Since the acoustic analysis on the powertrain was performed on each component separately due to computational capacity, the response cannot be accurately compared between test and CAE. Valleys due to overlap of different component anti-resonance frequencies are noticeable at similar speeds in the test data, i.e., at 2200 RPM in order 27, although valleys due to anti-resonance frequencies of each subcomponent may not be visible due to involvement of resonance in other components, as seen at 2500 RPM in order 54. This approach does not accurately depict the system's behavior but is a good indicator of overall noise levels from the orders.

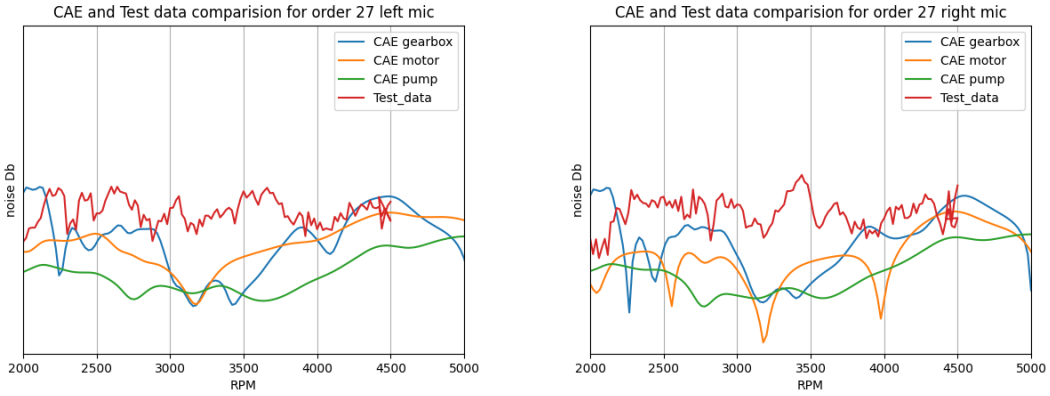

(a) Left mic **(b)** Right mic

Figure 4.1: Noise Response for order 27

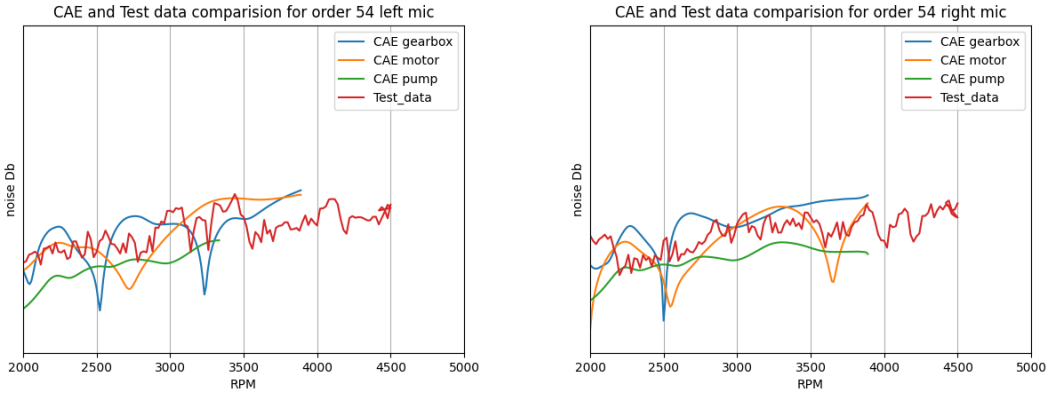

(a) Left mic **(b)** Right mic

Figure 4.2: Noise Response for order 54

4.1.1.2 Electric Motor Excitation Orders

The orders 8, 24, 32, and 48 associated with the harmonics of the motor are due to radial and tangential forces, and torque ripple excitations. Orders 8, 24, and 32 are influenced by radial and tangential forces, and orders 24 and 48 are influenced by torque ripple excitations.

Comparison of the CAE and test data suggests that orders relating to the torque ripple have a good corelation, but the magnitude is overestimated. The orders related to radial and tangential forces have a large deviation from the test data. In the case of order 8, this can be attributed to background noise. Deviation in order 32 may be caused because it coincides with hydraulic pulsation order 32.

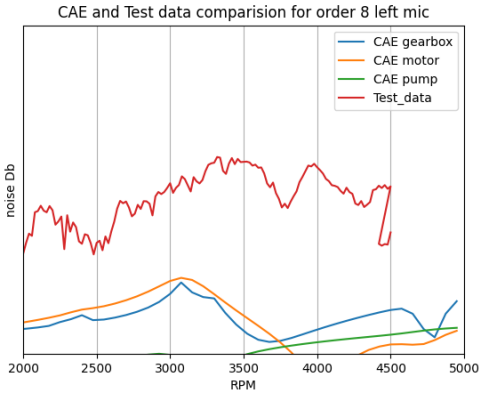

(a) Left mic

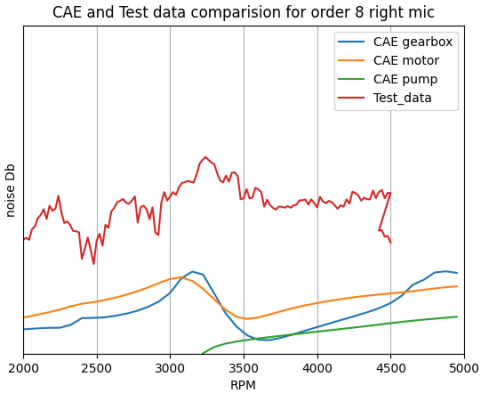

(b) Right mic

Figure 4.3: Noise Response for order 8

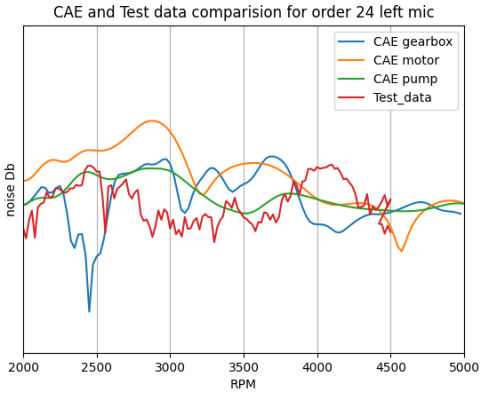

(a) Left mic

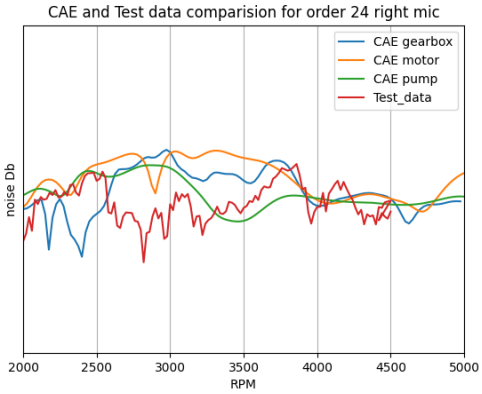

(b) Right mic

Figure 4.4: Noise Response for order 24

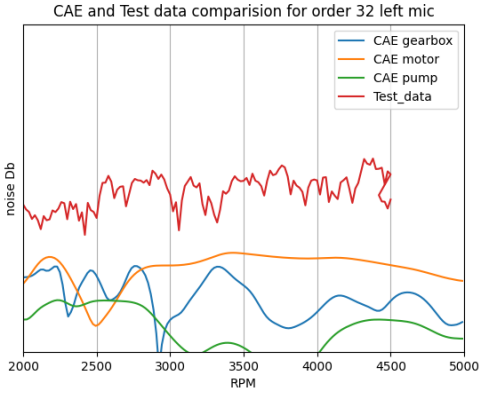

(a) Left mic

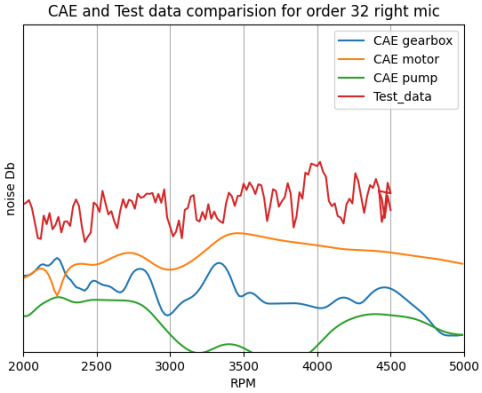

(b) Right mic

Figure 4.5: Noise Response for order 32

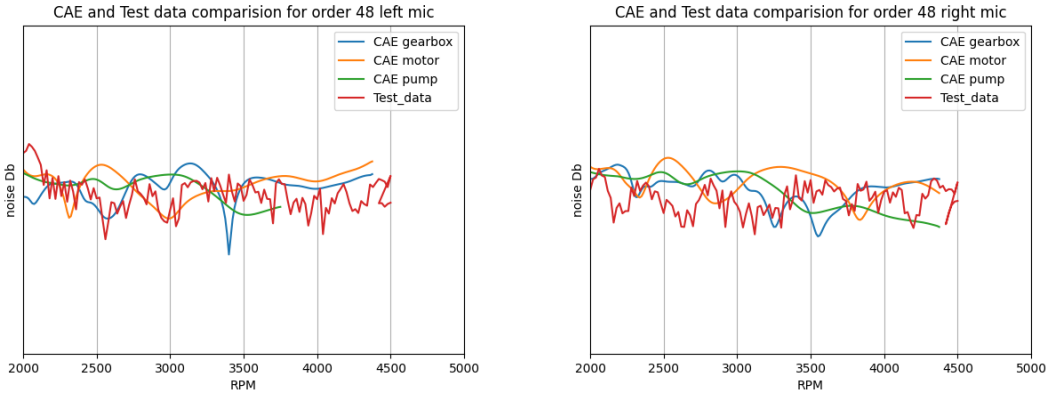

(a) Left mic **(b)** Right mic

Figure 4.6: Noise Response for order 48

4.1.2 Vibration

4.1.2.1 Gearbox Excitation Orders

The CAE vibration responses of orders 27, 54, and 81 have similar trends as in the case of test data. The CAE data and test data have better corelation on the nodes on top of the gearbox for gearbox excitation orders 27, 54, and 81, and similarly, corelation for the node on the electric motor is better for motor excitation orders 24 and 48, suggesting an error in the connection modeled between motor, gearbox, and pump FE components. In figure 4.10, the responses of orders 27, 54, and 81 relating to the gearbox excitations are compared in the frequency domain. In figure 4.10a, as expected from CAE data, the peaks of all three harmonics lie on the same frequencies, but in the case of measured data, as seen in figure 4.10b, the peaks of the harmonics tend to shift away from each other, and it is also noticeable that the shift is larger in higher frequencies. This explains why order 27 has a better corelation and orders 54 and 81 have a large difference between the speeds at which the peaks occur. The figure 4.11 compares the gearbox orders 27, 54, and 81 with hydraulic orders 28.8, 54.5, and 80. These lie very close to each other. The gearbox response have harmonics similar to hydraulic orders; this may have been due to order slicing bandwidth. The hydraulic orders lie in the bandwidth, which explains the additional peaks present in the test data that are absent in the CAE data.

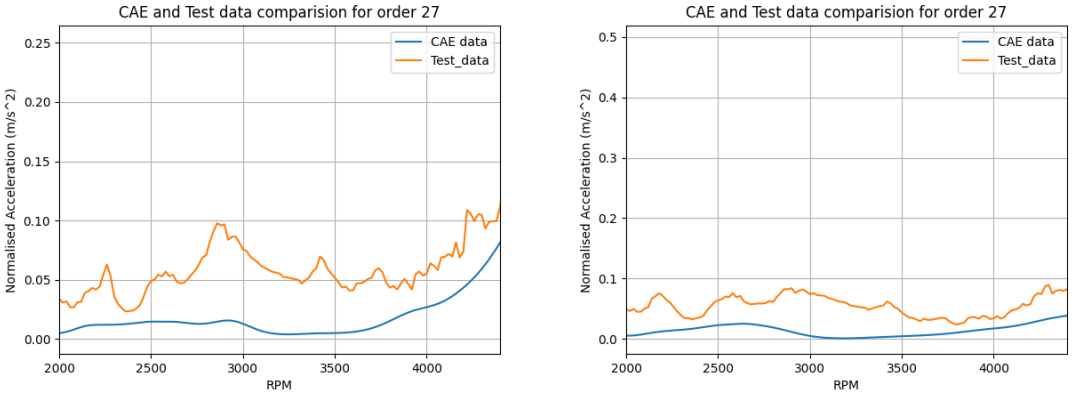

(a) Node on the top of gearbox **(b)** Node on the electric motor

Figure 4.7: Acceleration response for order 27

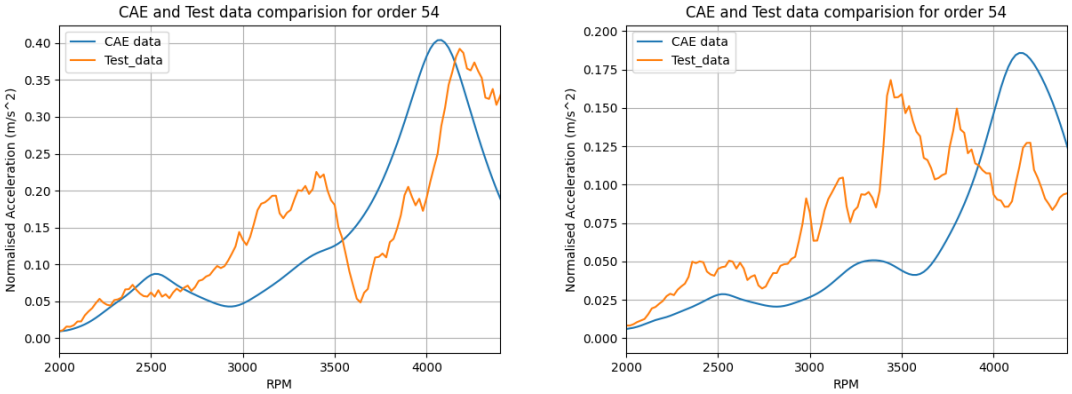

(a) Node on the top of gearbox **(b)** Node on the electric motor

Figure 4.8: Acceleration response for order 54

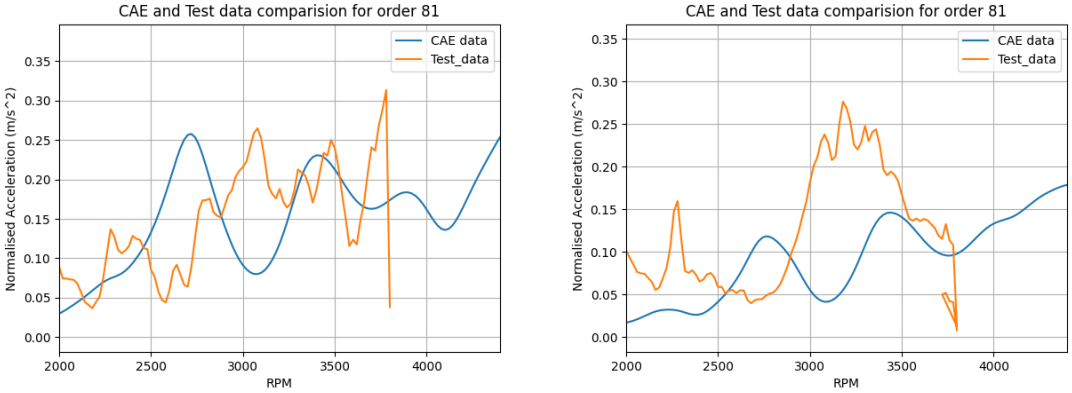

(a) Node on the top of gearbox **(b)** Node on the electric motor

Figure 4.9: Acceleration response for order 81

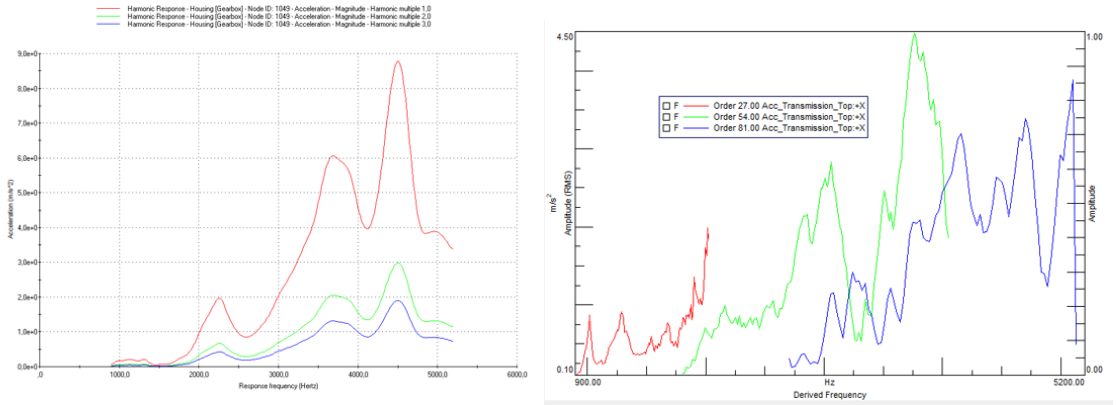

(a) CAE Gearbox orders **(b)** Test Gearbox orders

Figure 4.10: Gearbox Orders at gearbox top node comparison in frequency domain

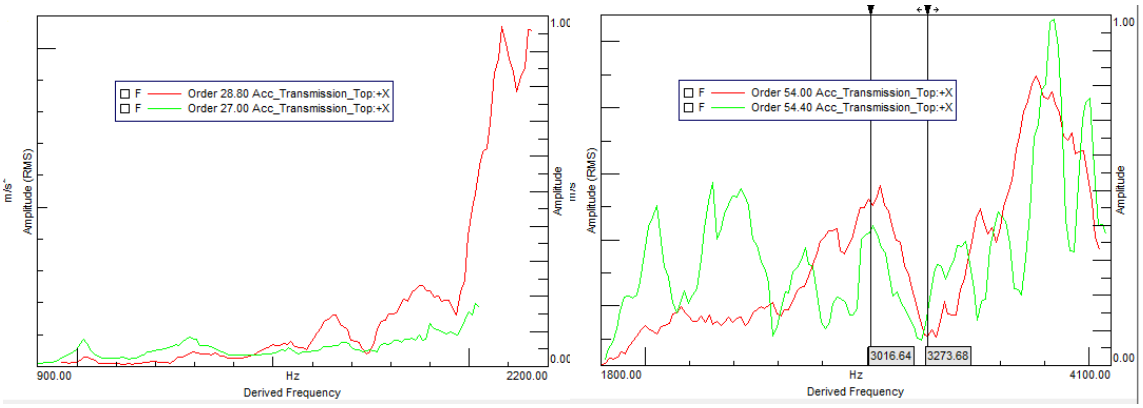

(a) Order 27 **(b)** Order 54

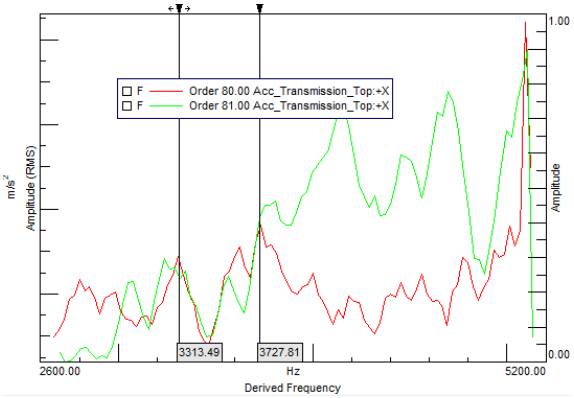

(c) Order 81

Figure 4.11: Harmonics of hydraulic orders in gearbox orders in frequency domain

4.1.2.2 Electric Motor Excitation Orders

Orders 8 and 32 relate to the radial and tangential excitations from the motor, and orders 24 and 48 relate to the torque ripple. The orders 8 and 32 have a high deviation from the test data. In the case of order 8, the response amplitude is low, and the deviation may have been influenced by background noise. In the case of order 32, the deviation may have been influenced by the order coinciding with the hydraulic pulsation order 32, as seen in figure 4.16a, order 32 has peaks similar to hydraulic order 28.8. Orders 24 and 48 have better corelation at the response node above the motor, with peaks matching at similar speeds. Order 24 is overestimated in the CAE data, as seen in figure 4.13 but order 48 has a better corelation despite it coinciding with hydraulic pulsation order 48.

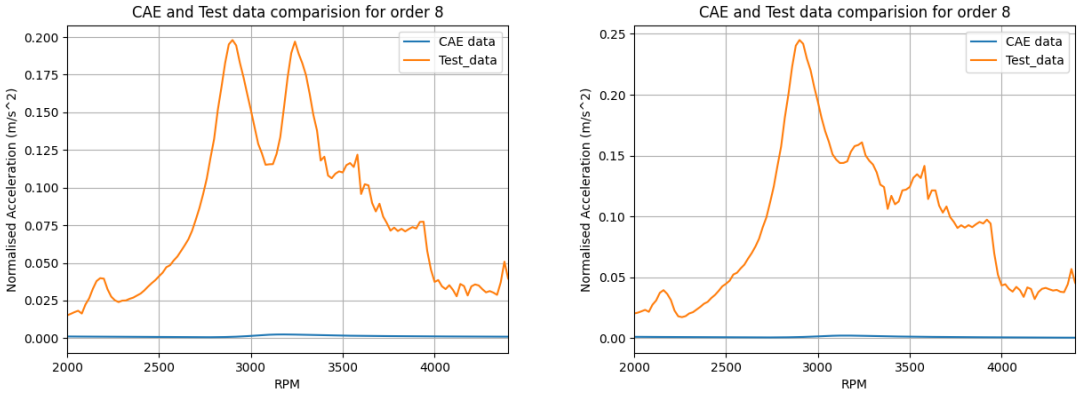

(a) Node on the top of gearbox **(b)** Node on the electric motor

Figure 4.12: Acceleration response for order 8

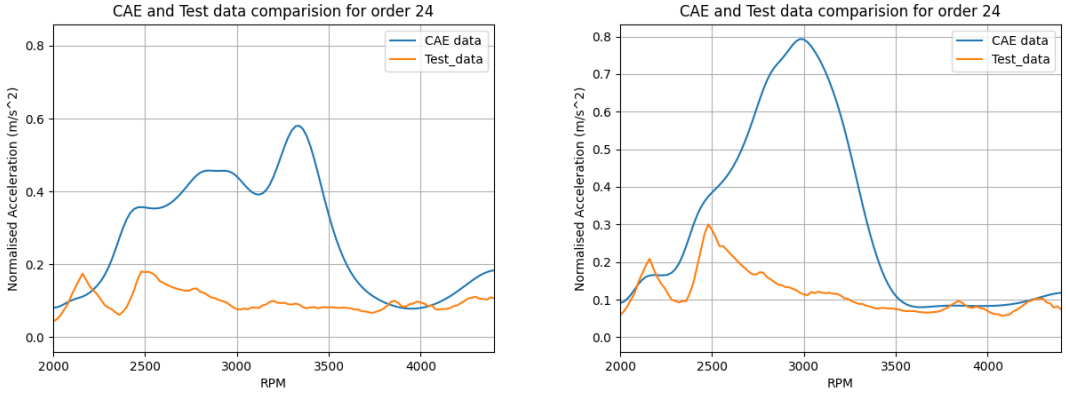

(a) Node on the top of gearbox **(b)** Node on the electric motor

Figure 4.13: Acceleration response for order 24

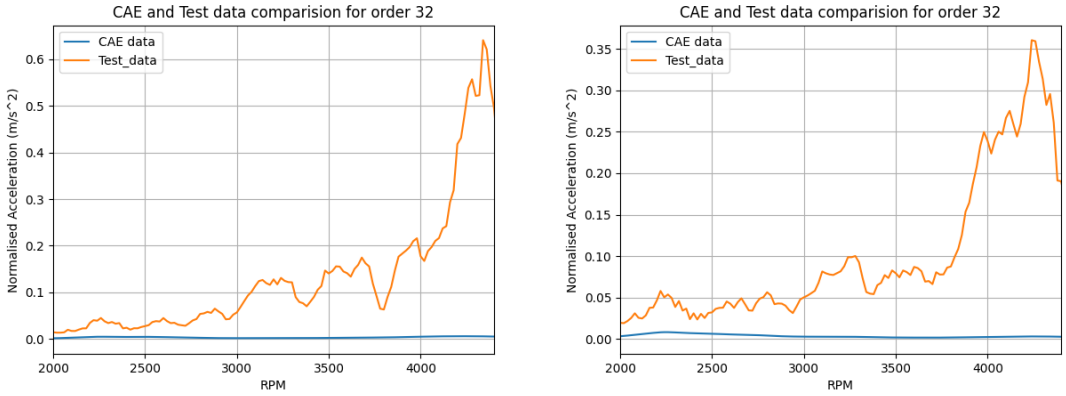

(a) Node on the top of gearbox **(b)** Node on the electric motor

Figure 4.14: Acceleration response for order 32

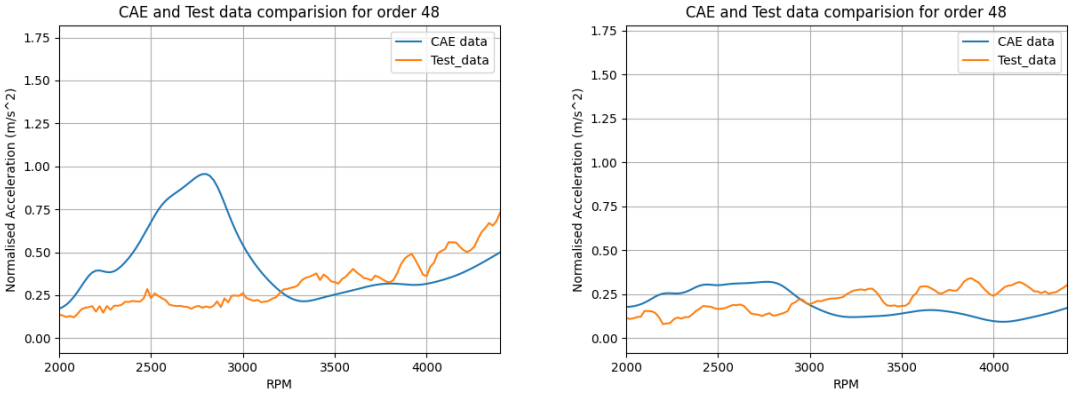

(a) Node on the top of gearbox **(b)** Node on the electric motor

Figure 4.15: Acceleration response for order 48

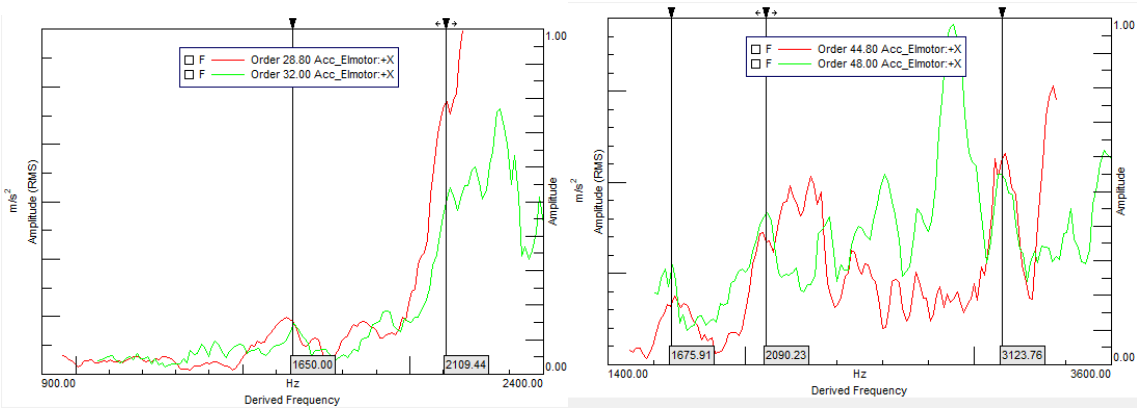

(a) Order 32 **(b)** Order 48

Figure 4.16: Harmonics of hydraulic orders in motor excitation orders in frequency domain

5
Conclusion

The study aimed to analyze and compare the CAE model built in ROMAX with the experimental data for the powertrain. In an ideal situation, the conditions of the CAE model and the test data would be similar, with the test rig free from background noise and vibration. Since the CAE model does not include the hydraulic pump dynamics, the damping from the transmission fluid and hydraulic oils, A deviation between the CAE and test data is expected.

The comparison between the NVH response of the powertrain obtained from the ROMAX model and experimental data yields comparable results. The ROMAX model demonstrated good correlation with the experimental data for the gearbox excitations. However, for the NVH response from torque ripple, the ROMAX model tended to overestimate the response, even though the peaks in the response align with those in the experimental data. Conversely, the NVH response from the motor's radial and tangential forces was underestimated in the ROMAX model. These observations suggest that the ROMAX model of the powertrain provides a reasonable approximation of NVH response, although fine-tuning the model to better represent the experimental data would yield better results.

6
Future Work

In this study the focus was limited to comparison and understanding the key differences in the CAE model and the test data. For future work on the topic and to better co-relate the test data with the CAE data following topics can be explored.

- NVH response of the Hydraulic pump are higher than that from the gearbox. Modelling the dynamics of the hydraulic pump and inclusion of hydraulic pulsation orders into the CAE model.
- Including the damping from individual systems and components into the CAE model.
- Influence of temperature variation on the system, and the influence it has on the NVH behaviour of the system.
- Study on perceived noise and vibration from the powertrain would help better understand the frequencies causing fatigue and annoyance for the occupants.
- Study the effect of wear on the NVH characteristics on the powertrain.

Bibliography

[1] In: (). URL: https://www.volvogroup.com/en/sustainable-transportation/responsible-business/climate.html#:~:text=Our%20ambition%20is%20to%20reach%20net%2Dzero%20value%20chain%20emissions,should%20have%20net%2Dzero%20emissions..

[2] In: (). URL: https://www.volvoce.com/europe/en/products/electric-machines/ec230-electric/.

[3] In: (). URL: https://www.ansys.com/products/electronics/ansys-maxwell.

[4] Blickensdorff J Boulliung M Burkard M Dold C Emretsson BG Genuit K Graf B Kurch M Millithaler P Mohr C Nichols M Pecher A Richter M Rittgerott T Satzinger S Stretz D Ulz A. Akustik. "Elektrifizierung des Antriebsstrangs, Berlin, Heidelberg." In: (). URL: https://doi.org/10.1007/978-3-662-60356-7_20.

[5] Ha T-W Huh J-W Choi S-K Min D-W. "Robust Development of Electric Powertrain NVH for Compact Electric SUV". In: *SAE Technical Paper 2020-01-1503, 2020* (2020). URL: doi:10.4271/2020-01-1503.

[6] ANUJIT DAFLE. "NVH analysis and optimization of an electric powertrain". In: (2022). URL: urn:nbn:se:kth:diva-320878.

[7] Michon M Holehouse R Shahaj A Jafarali H. "System Interactions Affecting NVH Performance of an Electric Vehicle Drivetrain". In: *SAE Technical Paper 2019-01-1545* (2019). URL: https://doi.org/10.4271/2019-01-1545.

[8] Devillers E Degrendele K Hecquet M Lecointe J-P. "Open-Access Testbench Data for NVH Benchmarking of E-machines under Electromagnetic Excitations". In: *SAE Technical Paper 2019-01-1459, 2019* (2019). URL: doi:10.4271/2019-01-1459..

[9] Gavric L. "NVH refinement issues for BEV". In: (2020). URL: https://doi.org/10.1007/978-3-658-27669-0_1.

[10] Holehouse R Shahaj A Michon M and James B. "Integrated Approach to Electro-Mechanical System NVH analysis". In: *SAE Technical Paper No. 2018-01-1499* (2020). URL: https://www.sae.org/publications/technical-papers/content/2018-01-1499/.

[11] Janda Marcel and Jandova Kristyna. "Vibration Simulation of Electric Machines". In: Feb. 2018. ISBN: 978-953-51-3849-5. DOI: 10.5772/intechopen.72266.

[12] Åkerblom Mats. "Gear Noise and Vibration: A Literature Survey". In: (2001). URL: urn:nbn:se:kth:diva-9891.

[13] "MotorCAD". In: (). URL: https://www.motor-design.com/motor-cad/.

[14] Senousy M Larsen P and Ding P. “Electromagnetics, Structural Harmonics and Acoustics Coupled Simulation on the Stator of an Electric Motor”. In: *SAE Int. J. Passeng. Cars - Mech. Syst* (2014). URL: doi:10.4271/2014-01-0933..

[15] Maria Antonietta Panza. “A Review of Experimental Techniques for NVH Analysis on a Commercial Vehicle”. In: *Energy Procedia* 82 (2015). 70th Conference of the Italian Thermal Machines Engineering Association, ATI2015, pp. 1017–1023. ISSN: 1876-6102. DOI: https://doi.org/10.1016/j.egypro.2015.11.861. URL: https://www.sciencedirect.com/science/article/pii/S1876610215026211.

[16] Alexander Petrovsky et al. “Digital order tracking analysis for rotating machinery monitoring. Theory and implementation”. In: (Jan. 2008).

[17] “PMSM motor”. In: (). URL: https://en.engineering-solutions.ru/motorcontrol/pmsm/.

[18] Dupont J Aydoun R and Bouvet P. “Simulation of the Noise Radiated by an Automotive Electric Motor: Influence of the Motor Defects”. In: *SAE Int. J.Alt. Power* (2014). URL: doi:10.4271/2014-01-2070.

[19] “ROMAX”. In: (). URL: https://romaxtech.com/events-and-resources/news/announcing-romax-2022-1/.

[20] “Siemens Simcenter Testlab”. In: (). URL: https://plm.sw.siemens.com/en-US/simcenter/physical-testing/testlab/.

[21] VIGNESH SUBRAMANIAN. “NVH analysis and optimization of an electric powertrain”. In: (2022). URL: https://hdl.handle.net/20.500.12380/305055.

[22] Zhang H Jaura A Kumar D Sambharam T. “Multiphysics Simulation of Electric Motor NVH Performance with Eccentricity”. In: *SAE Technical Paper 2021-01-1077, 2021* (2021). URL: doi:10.4271/2021-01-1077.

[23] “torque ripple”. In: (). URL: https://www.motioncontroltips.com/whats-the-difference-between-cogging-torque-and-torque-ripple/.

[24] “triaxial accelerometer”. In: (). URL: https://www.pcb.com/products?m=ht356b21.

[25] Anders Brandt Thomas Lagö Kjell Ahlin Jiri Tuma. “Main Principles and Limitations of Current Order Tracking Methods”. In: (2005). URL: http://www.sandv.com/downloads/0503bran.pdf.

[26] Parmar A Miskin A Maheswar Rao U and Reddy HK. “Simulation Diagnostics Approach for Identification, Ranking and Optimization of Electric Motor Design Parameters for Optimal NVH Performance”. In: *SAE Technical Paper 2021-01-1079, 2021* (2021). URL: doi:10.4271/2021-01-1079.

[27] “Understanding FFTs and Windowing”. In: (). URL: https://download.ni.com/evaluation/pxi/Understanding%20FFTs%20and%20Windowing.pdf.

[28] “VibeSys module in nCode”. In: (). URL: https://www.hbkworld.com/en/products/software/durability/ncode-vibesys-acoustic-and-vibration-analysis-software.

[29] Zhao W Liu Z Yang Y. “Improving the transmission error source tracing method for gear hobbing machines”. In: (). URL: https://journals.sagepub.com/doi/full/10.1177/16878140211072962.

A
Appendix 1

A.1 Load Case 1 100% load

A.1.1 Noise

A.1.1.1 Gearbox Excitation Orders

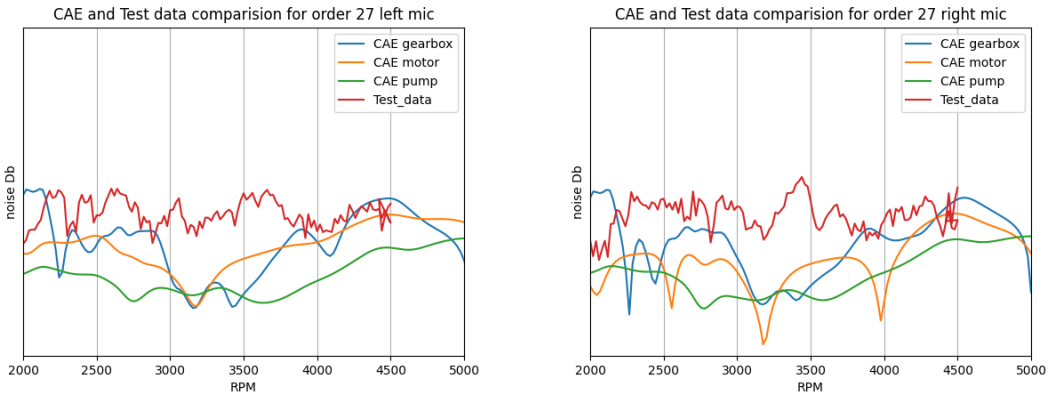

(a) Left mic **(b)** Right mic

Figure A.1: Noise Response for order 27

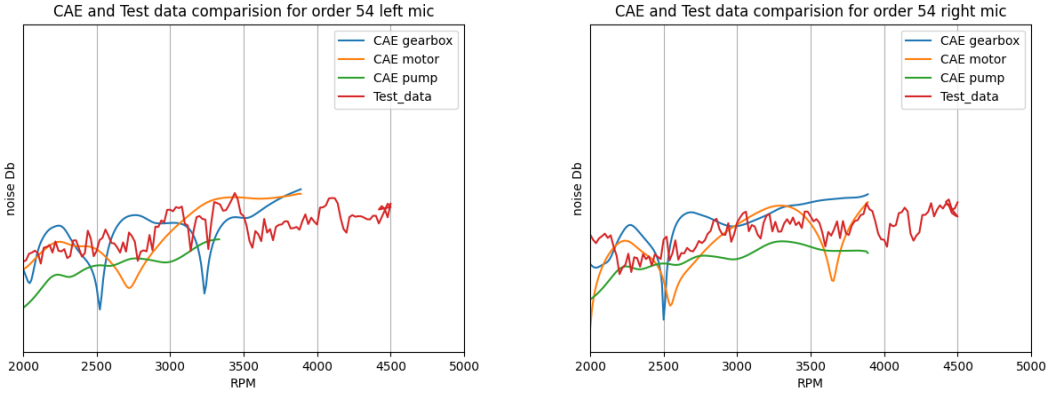

(a) Left mic **(b)** Right mic

Figure A.2: Noise Response for order 54

A.1.1.2 Electric Motor Excitation Orders

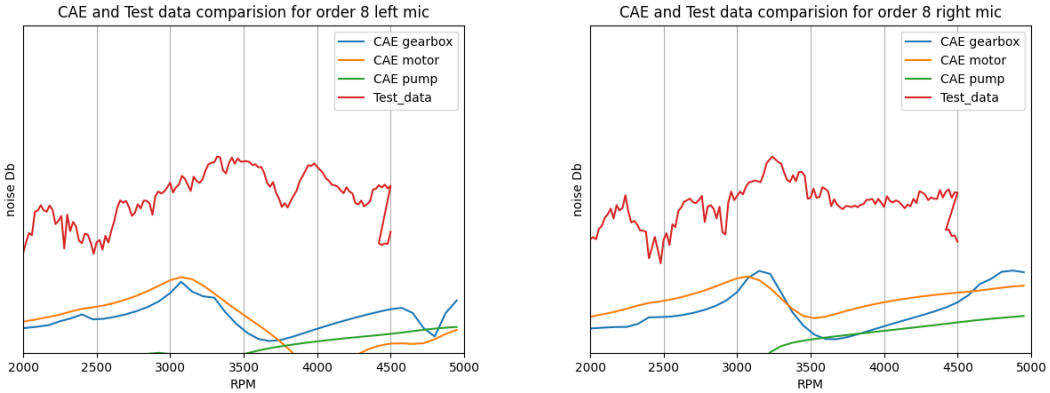

(a) Left mic **(b)** Right mic

Figure A.3: Noise Response for order 8

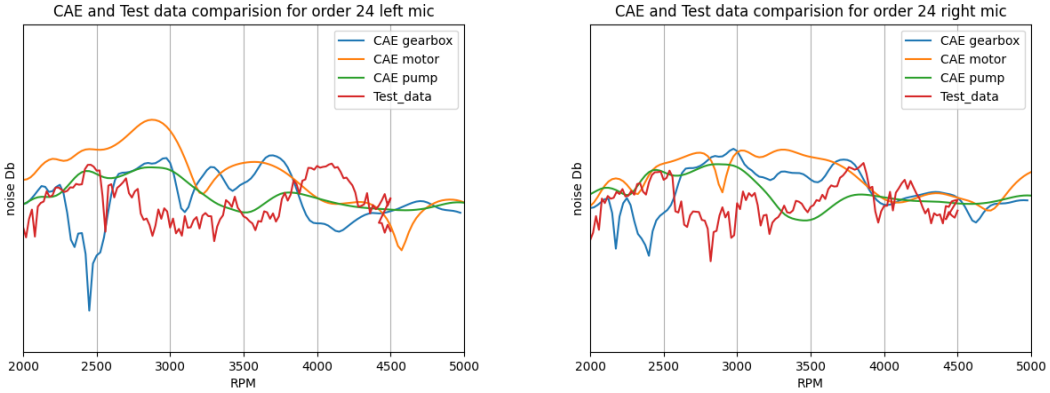

(a) Left mic **(b)** Right mic

Figure A.4: Noise Response for order 24

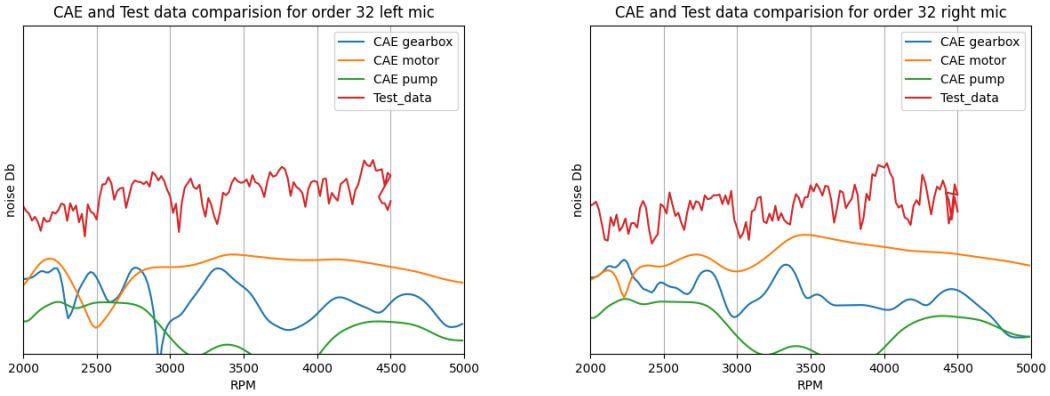

(a) Left mic **(b)** Right mic

Figure A.5: Noise Response for order 32

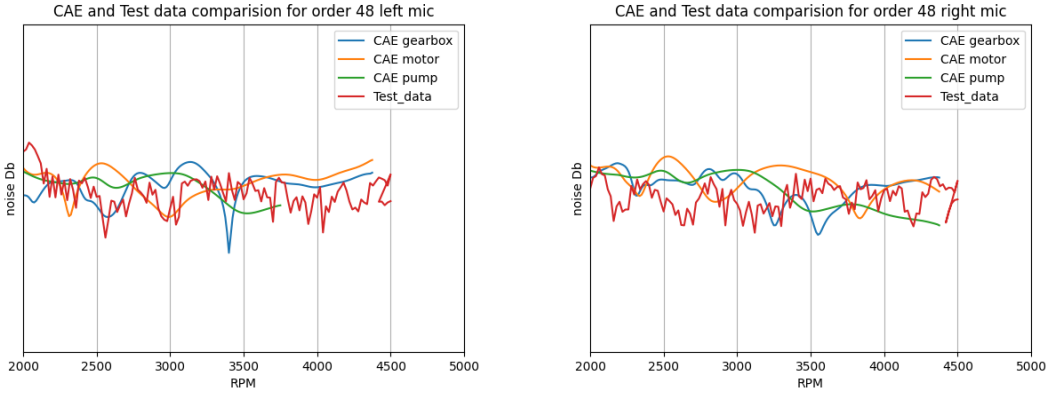

(a) Left mic **(b)** Right mic

Figure A.6: Noise Response for order 48

A.1.2 Vibration

A.1.2.1 Gearbox Excitation Orders

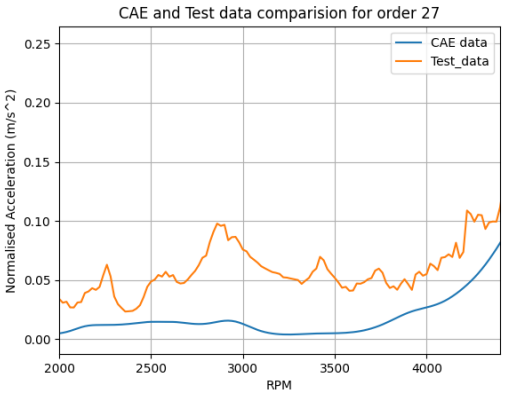

(a) Node on the top of gearbox

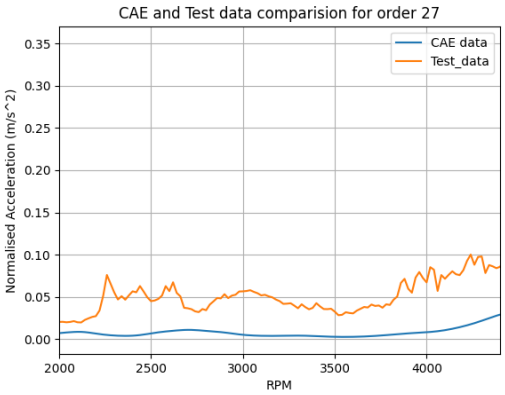

(b) Node on the side of gearbox

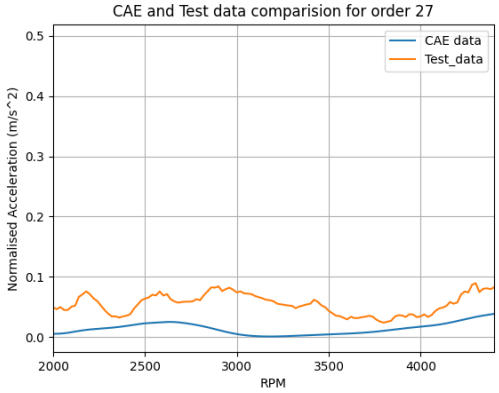

(c) Node on the electric motor

Figure A.7: Acceleration response for order 27

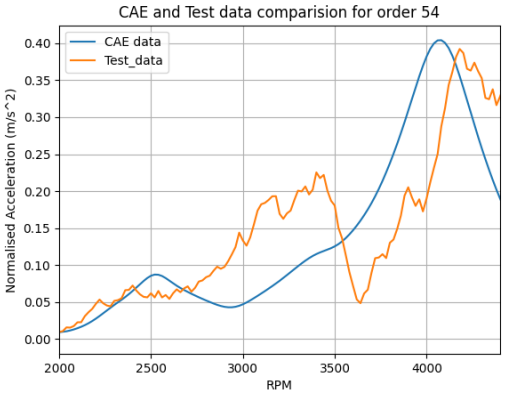

(a) Node on the top of gearbox

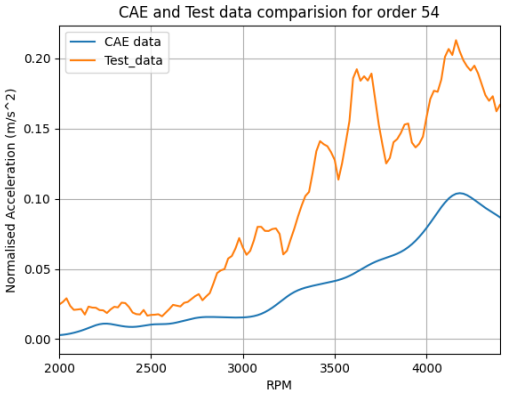

(b) Node on the side of gearbox

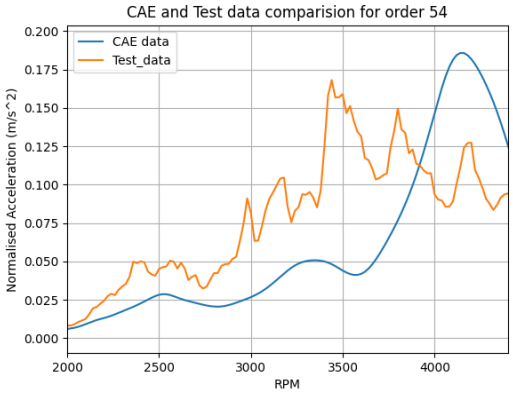

(c) Node on the electric motor

Figure A.8: Acceleration response for order 54

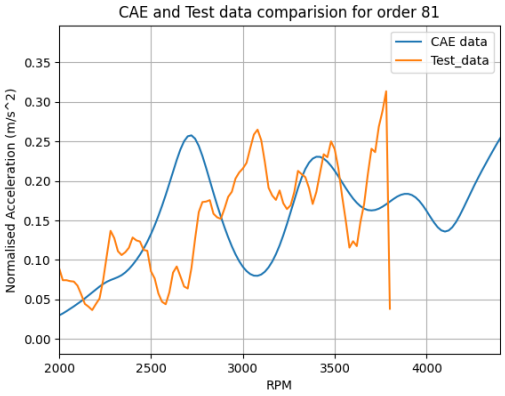

(a) Node on the top of gearbox

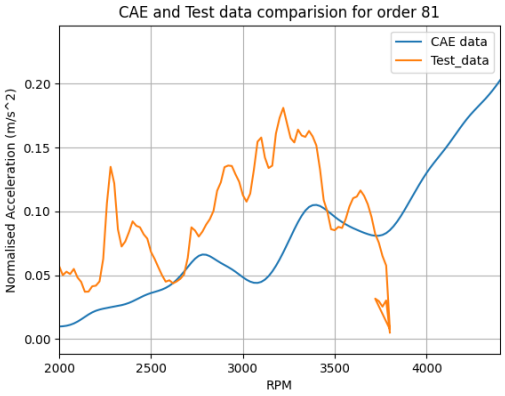

(b) Node on the side of gearbox

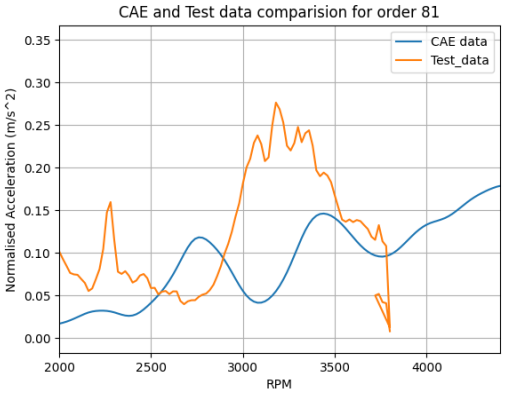

(c) Node on the electric motor

Figure A.9: Acceleration response for order 81

A.1.2.2 Electric Motor Excitation Orders

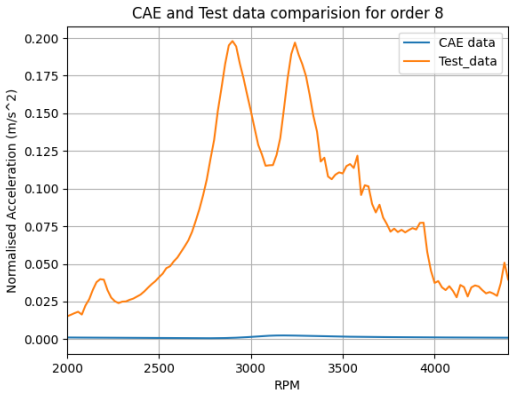

(a) Node on the top of gearbox

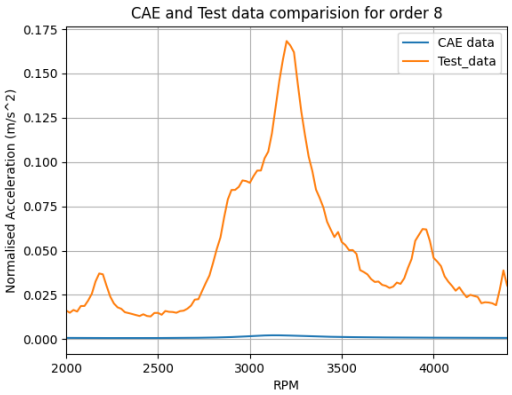

(b) Node on the side of gearbox

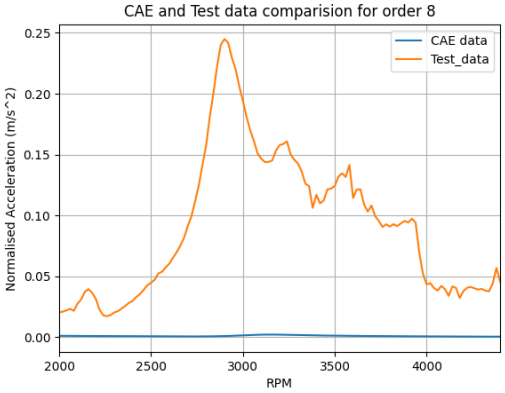

(c) Node on the electric motor

Figure A.10: Acceleration response for order 8

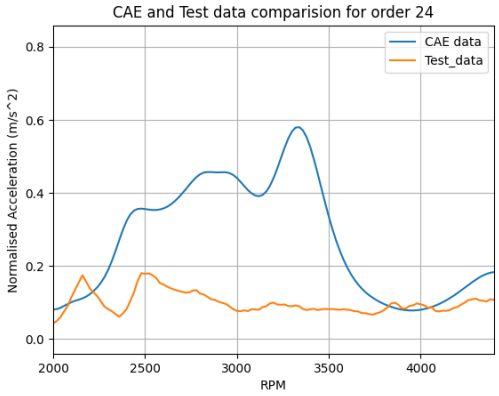

(a) Node on the top of gearbox

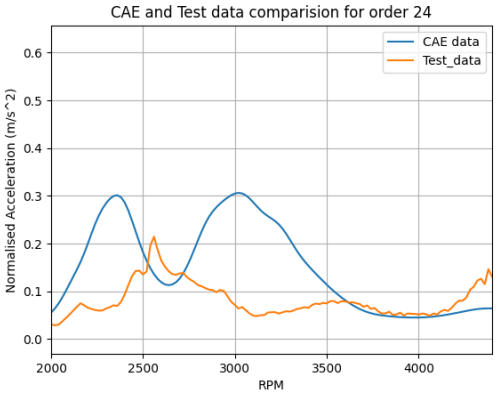

(b) Node on the side of gearbox

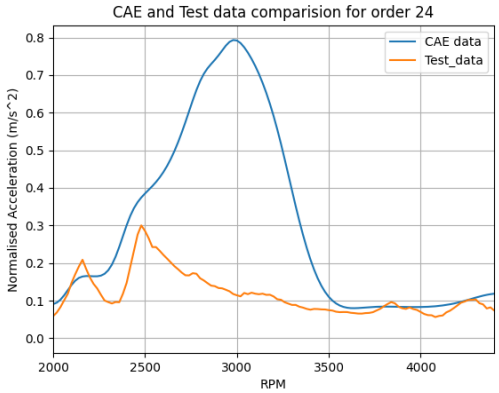

(c) Node on the electric motor

Figure A.11: Acceleration response for order 24

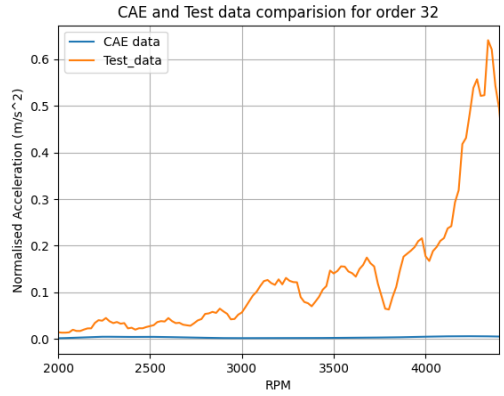

(a) Node on the top of gearbox

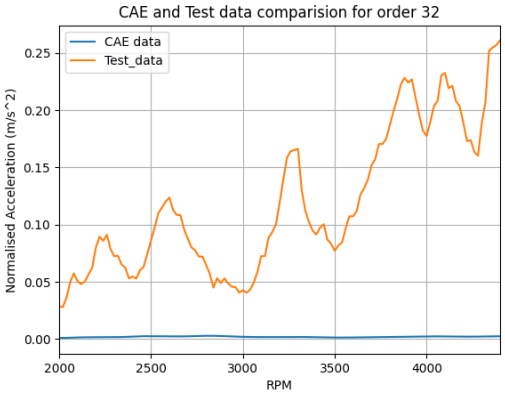

(b) Node on the side of gearbox

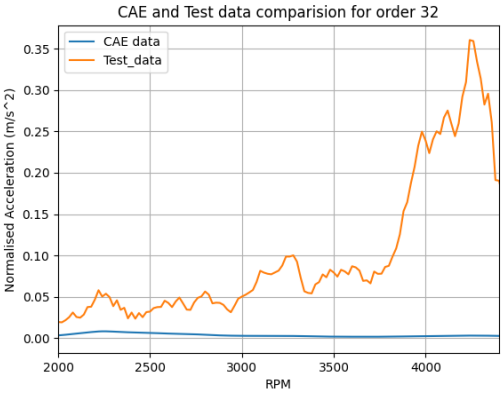

(c) Node on the electric motor

Figure A.12: Acceleration response for order 32

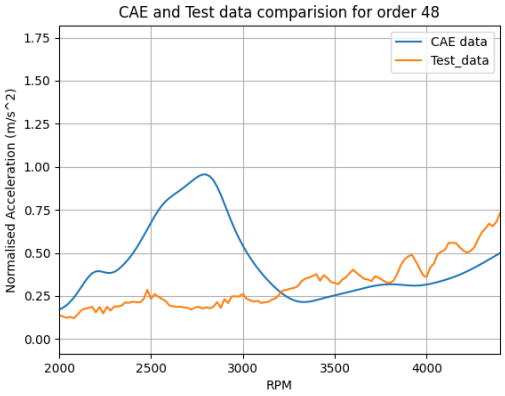

(a) Node on the top of gearbox

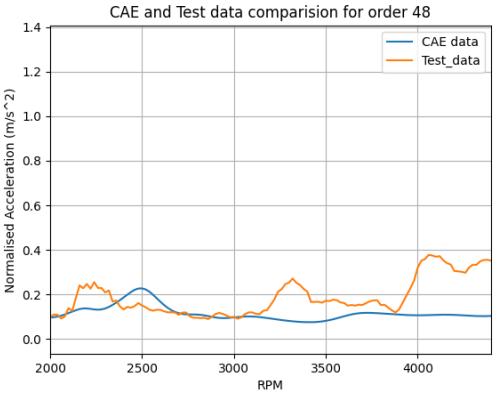

(b) Node on the side of gearbox

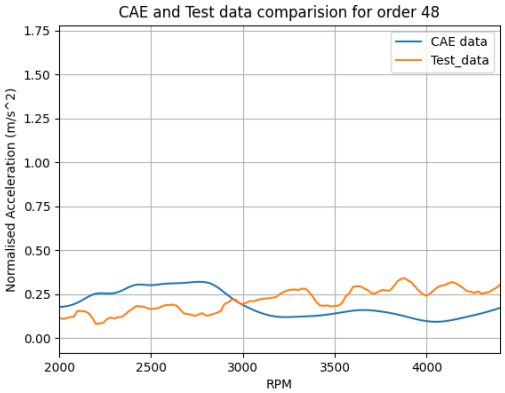

(c) Node on the electric motor

Figure A.13: Acceleration response for order 48

A.2 Load Case 2 50% load

A.2.1 Noise

A.2.1.1 Gearbox Excitation Orders

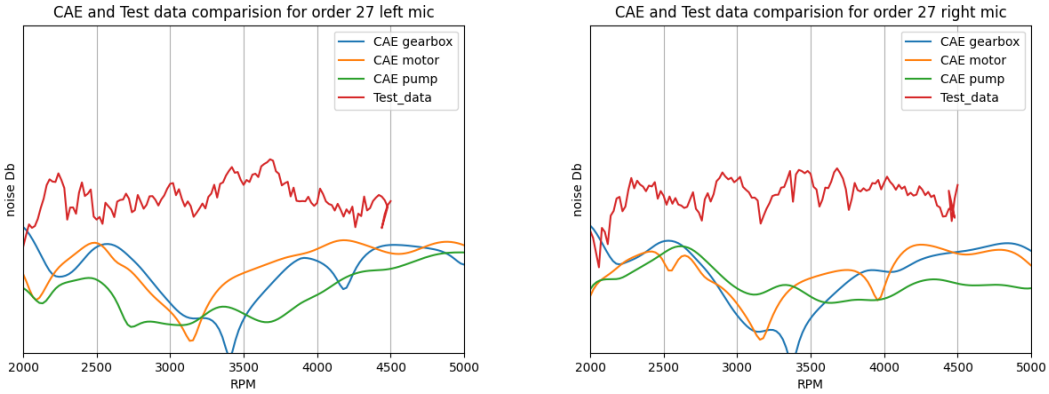

(a) Left mic **(b)** Right mic

Figure A.14: Noise Response for order 27

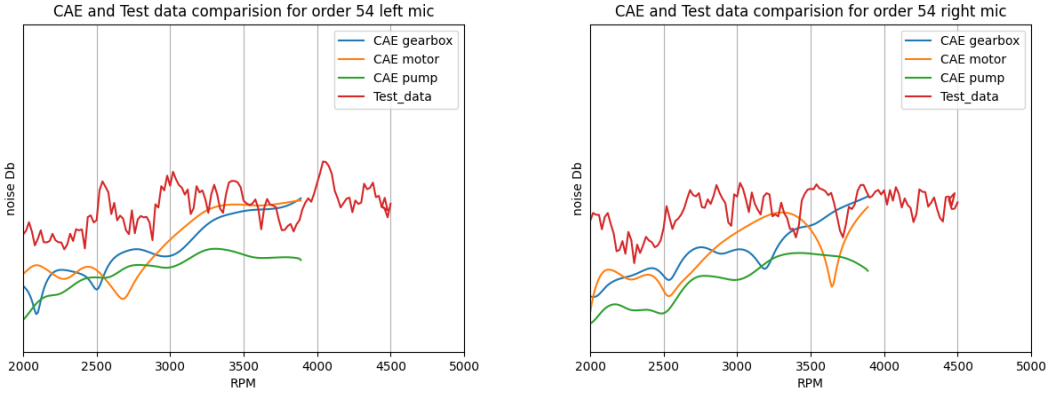

(a) Left mic **(b)** Right mic

Figure A.15: Noise Response for order 54

A.2.1.2 Electric Motor Excitation Orders

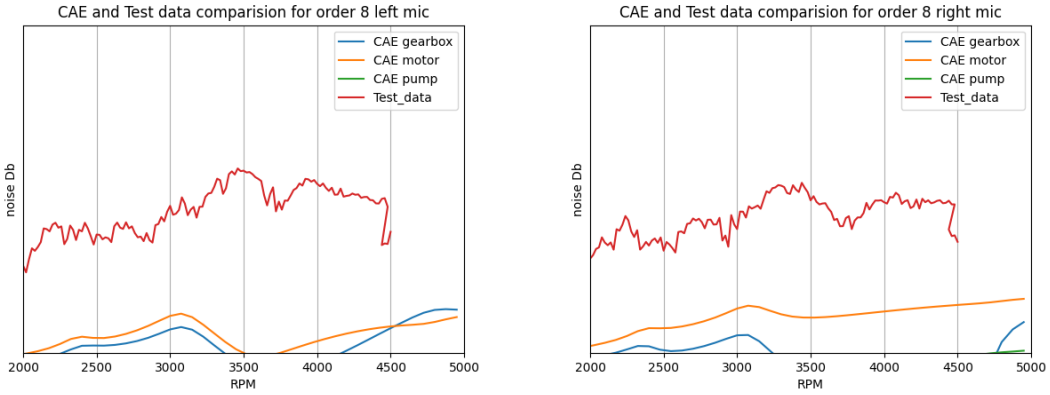

(a) Left mic **(b)** Right mic

Figure A.16: Noise Response for order 8

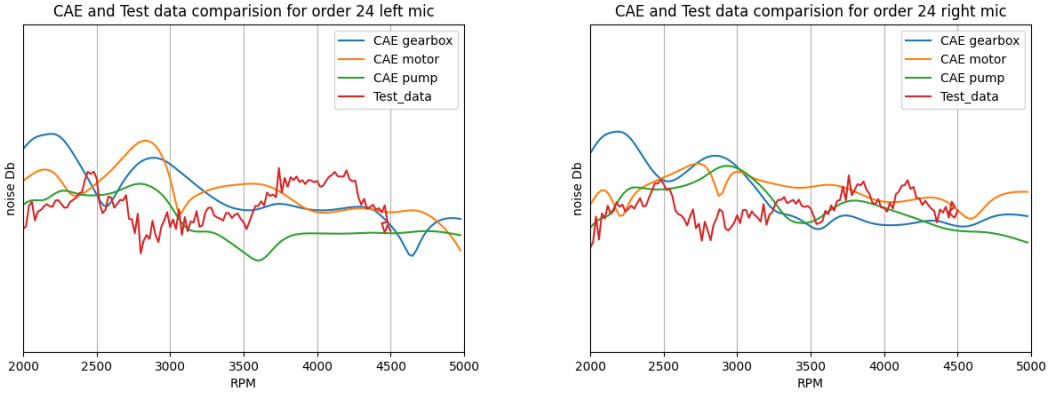

(a) Left mic **(b)** Right mic

Figure A.17: Noise Response for order 24

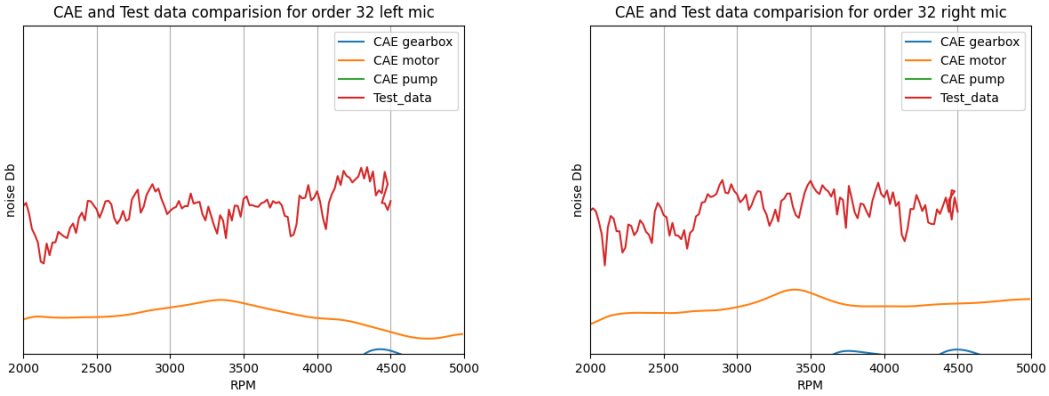

(a) Left mic **(b)** Right mic

Figure A.18: Noise Response for order 32

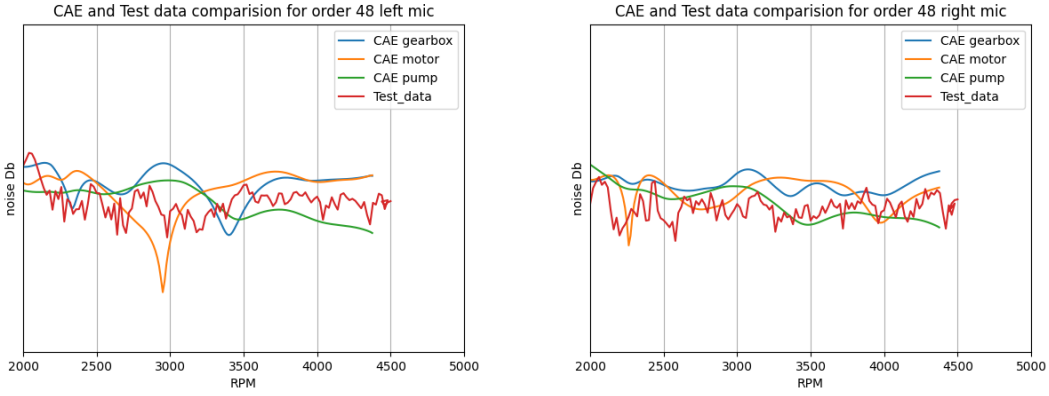

(a) Left mic **(b)** Right mic

Figure A.19: Noise Response for order 48

A.2.2 Vibration

A.2.2.1 Gearbox Excitation Orders

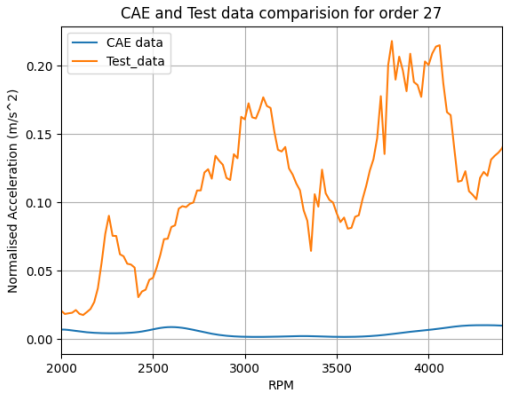

(a) Node on the top of gearbox

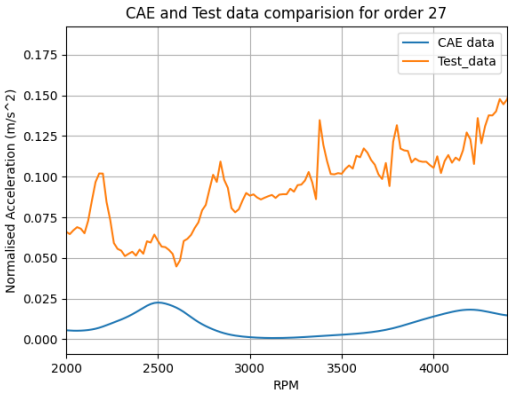

(b) Node on the side of gearbox

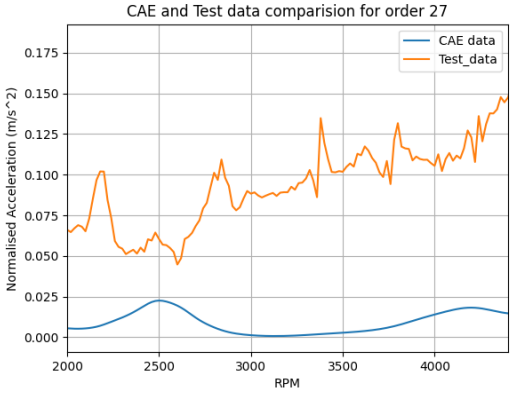

(c) Node on the electric motor

Figure A.20: Acceleration response for order 27

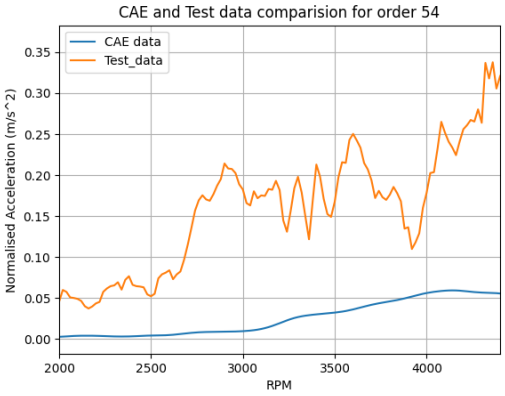

(a) Node on the top of gearbox

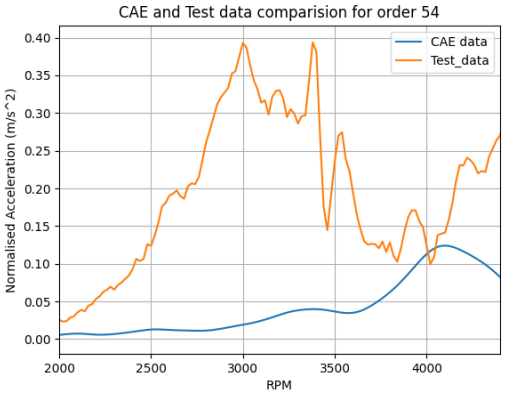

(b) Node on the side of gearbox

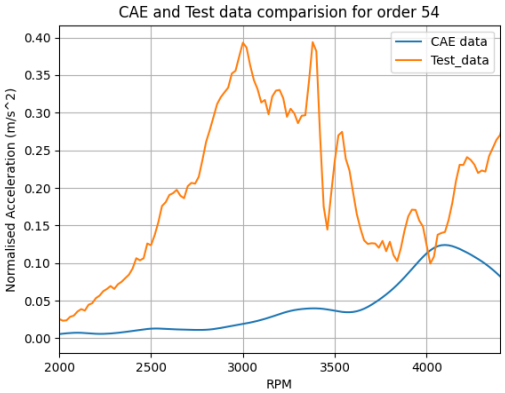

(c) Node on the electric motor

Figure A.21: Acceleration response for order 54

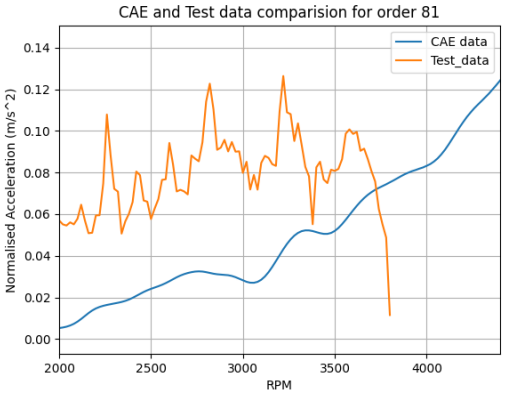

(a) Node on the top of gearbox

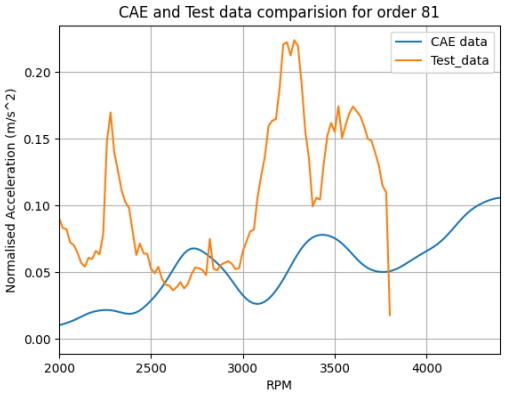

(b) Node on the side of gearbox

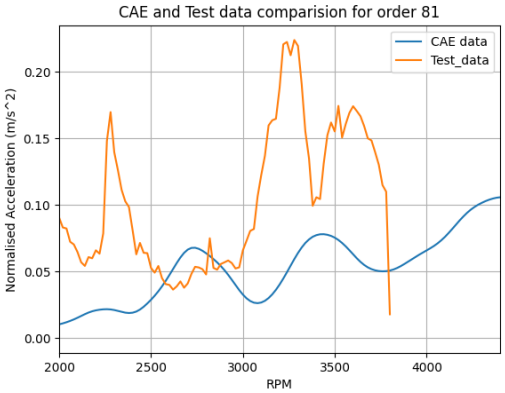

(c) Node on the electric motor

Figure A.22: Acceleration response for order 81

A.2.2.2 Electric Motor Excitation Orders

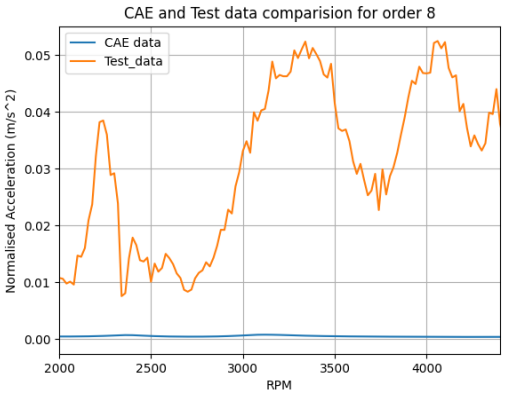

(a) Node on the top of gearbox

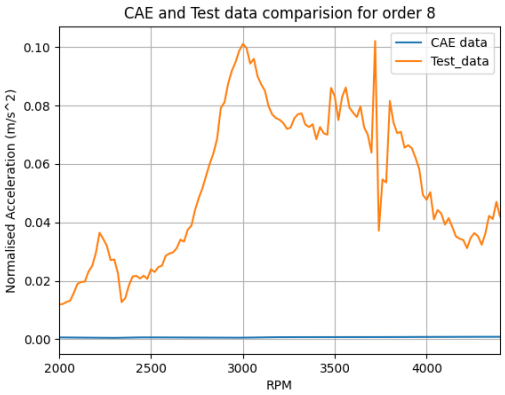

(b) Node on the side of gearbox

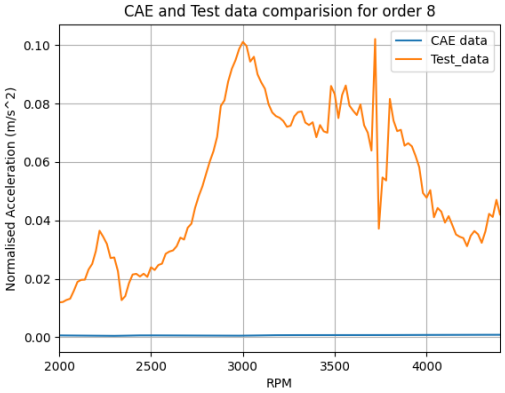

(c) Node on the electric motor

Figure A.23: Acceleration response for order 8

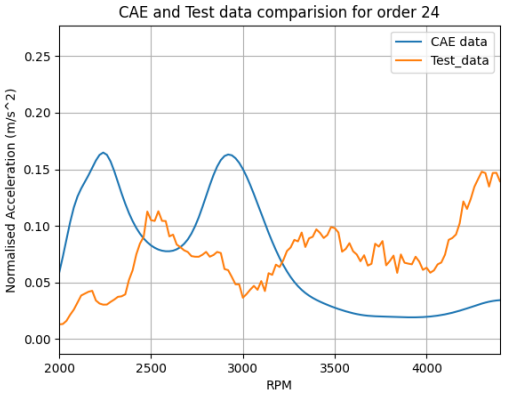

(a) Node on the top of gearbox

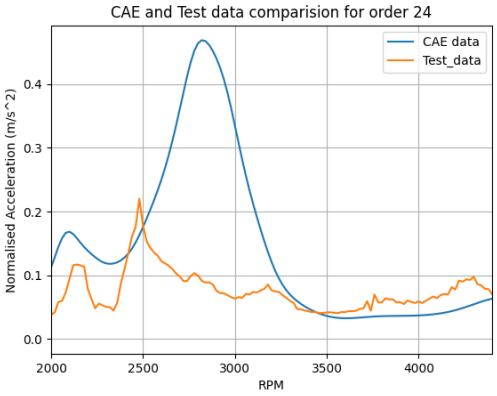

(b) Node on the side of gearbox

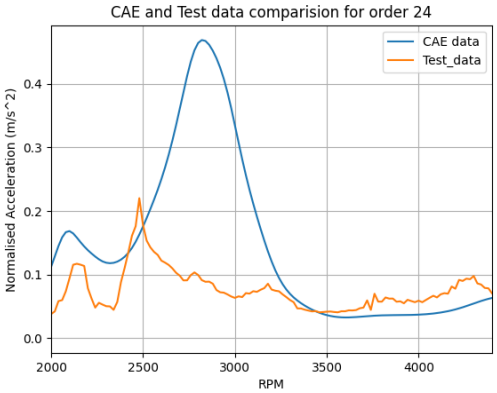

(c) Node on the electric motor

Figure A.24: Acceleration response for order 24

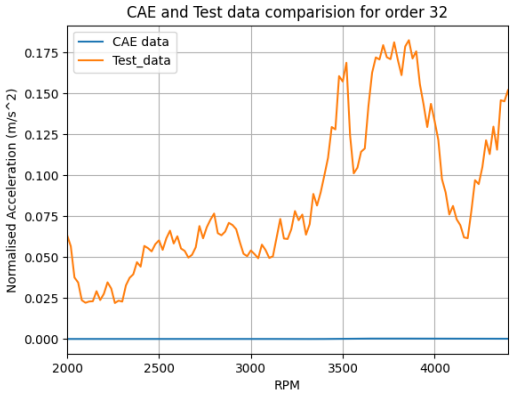

(a) Node on the top of gearbox

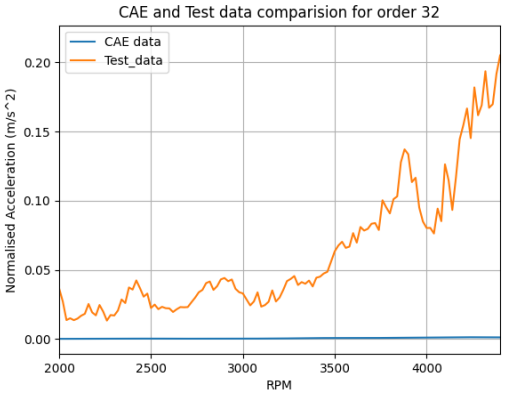

(b) Node on the side of gearbox

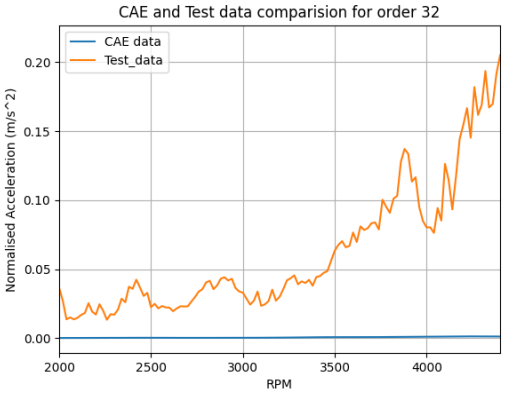

(c) Node on the electric motor

Figure A.25: Acceleration response for order 32

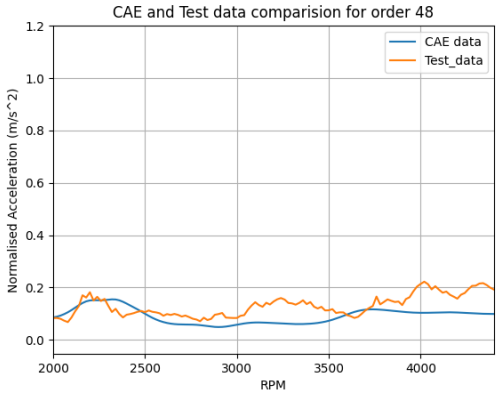

(a) Node on the top of gearbox

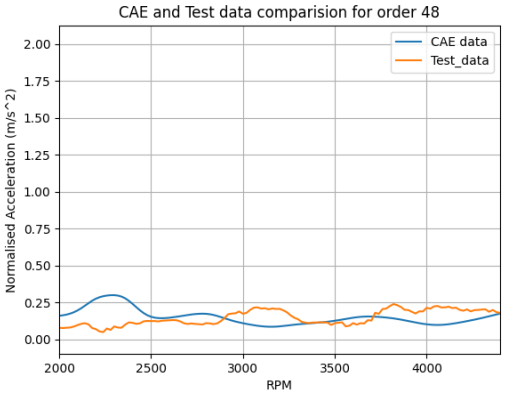

(b) Node on the side of gearbox

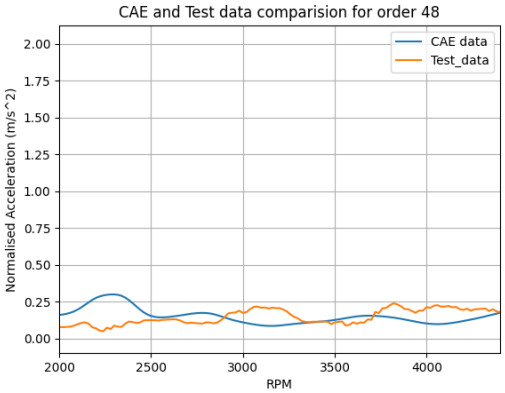

(c) Node on the electric motor

Figure A.26: Acceleration response for order 48

A.3 Load Case 3 25% load

A.3.1 Noise

A.3.1.1 Gearbox Excitation Orders

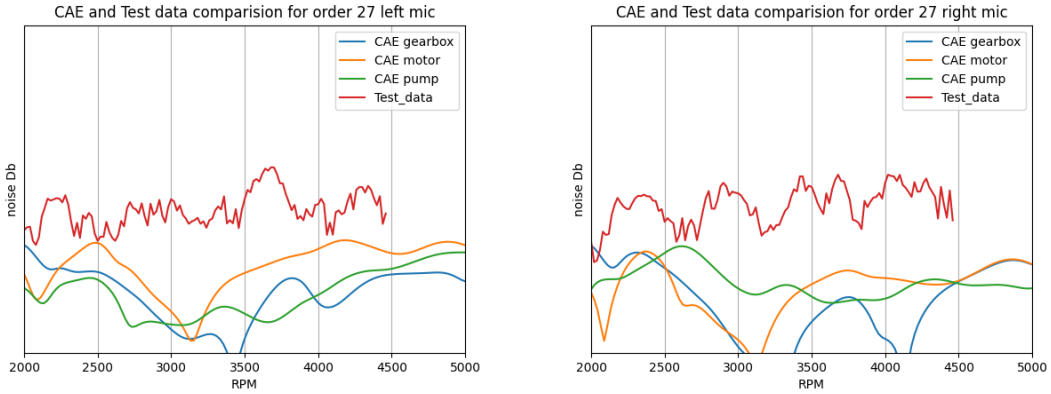

(a) Left mic **(b)** Right mic

Figure A.27: Noise Response for order 27

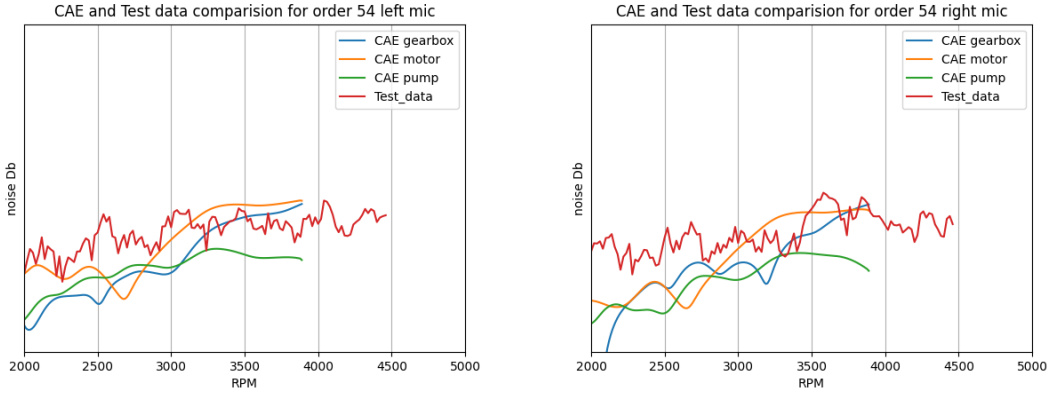

(a) Left mic **(b)** Right mic

Figure A.28: Noise Response for order 54

A.3.1.2 Electric Motor Excitation Orders

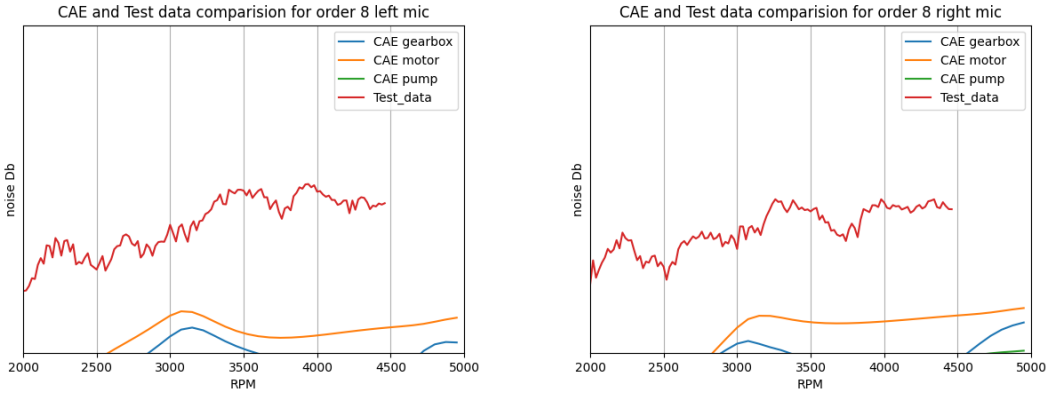

(a) Left mic **(b)** Right mic

Figure A.29: Noise Response for order 8

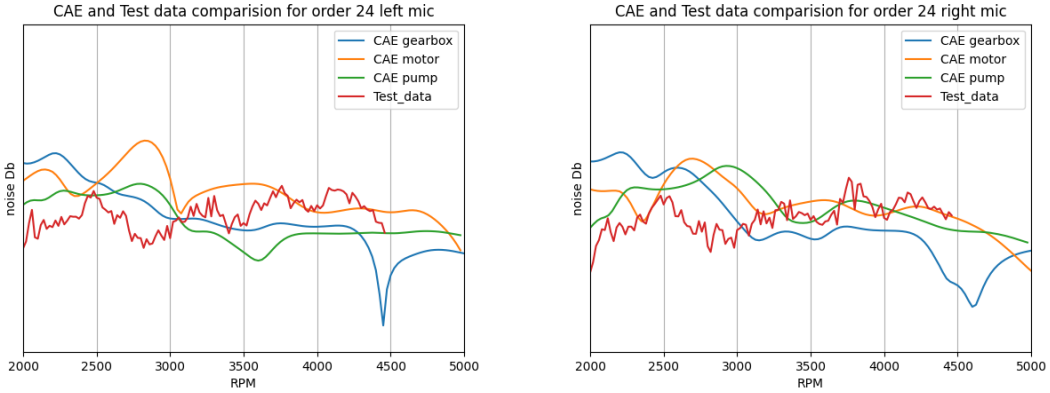

(a) Left mic **(b)** Right mic

Figure A.30: Noise Response for order 24

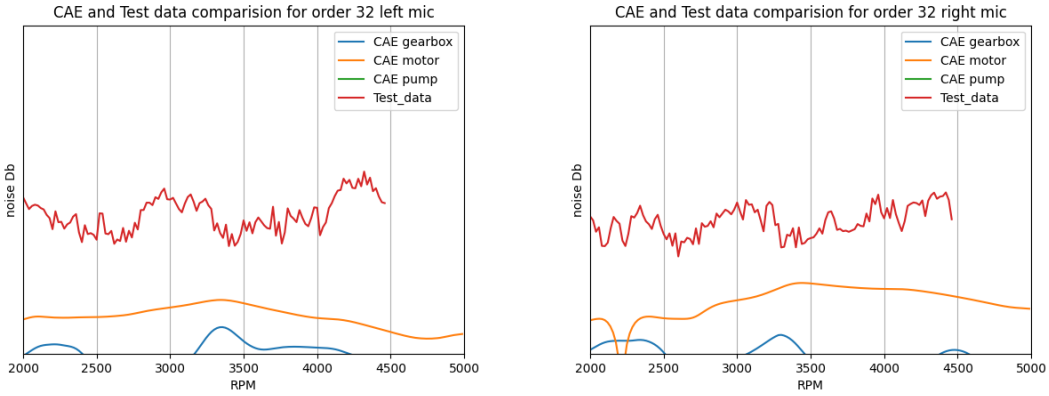

(a) Left mic **(b)** Right mic

Figure A.31: Noise Response for order 32

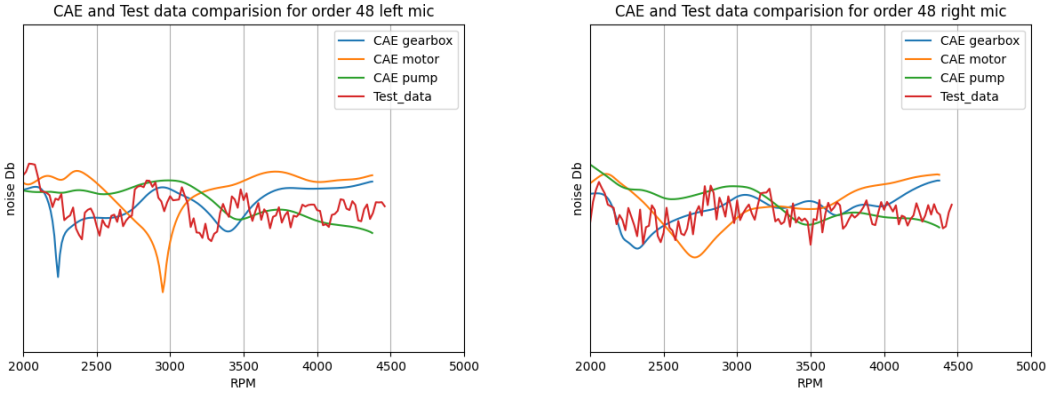

(a) Left mic **(b)** Right mic

Figure A.32: Noise Response for order 48

A.3.2 Vibration

A.3.2.1 Gearbox Excitation Orders

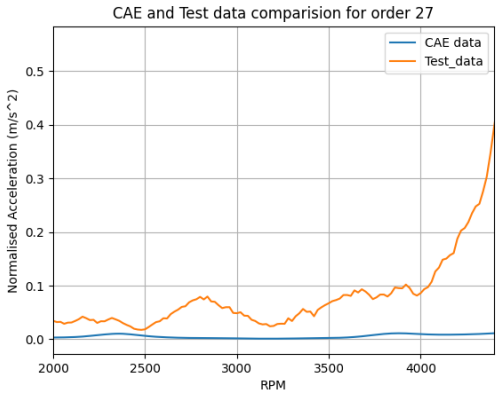

(a) Node on the top of gearbox

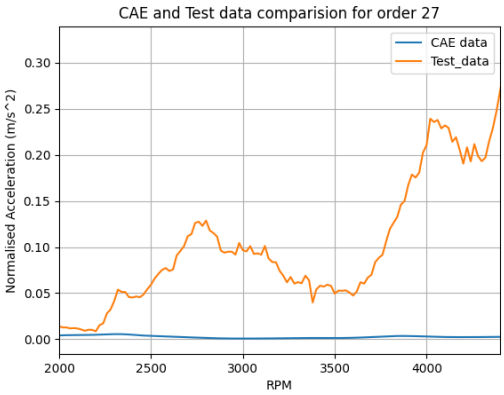

(b) Node on the side of gearbox

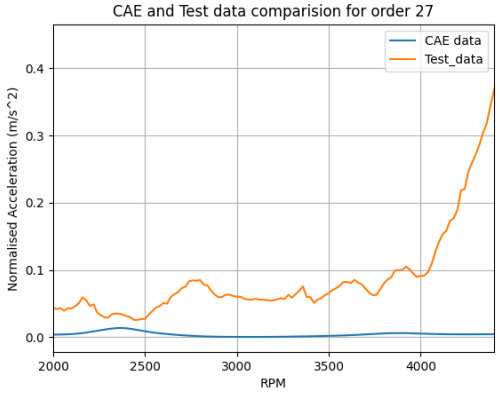

(c) Node on the electric motor

Figure A.33: Acceleration response for order 27

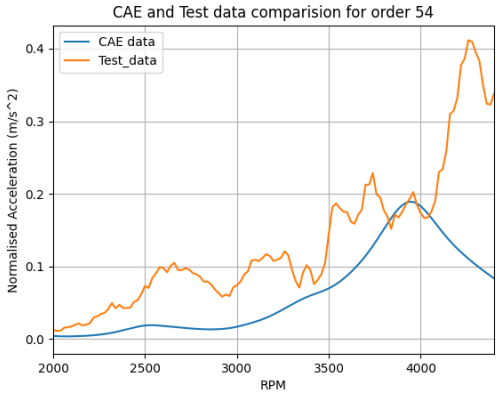

(a) Node on the top of gearbox

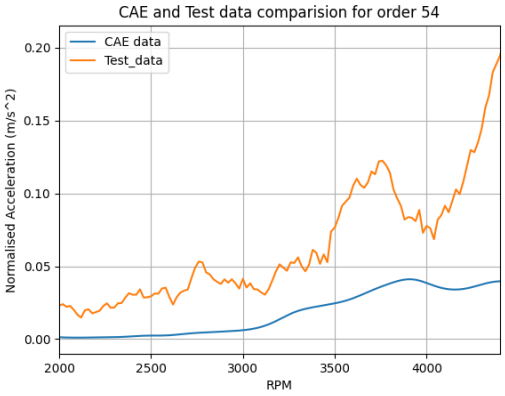

(b) Node on the side of gearbox

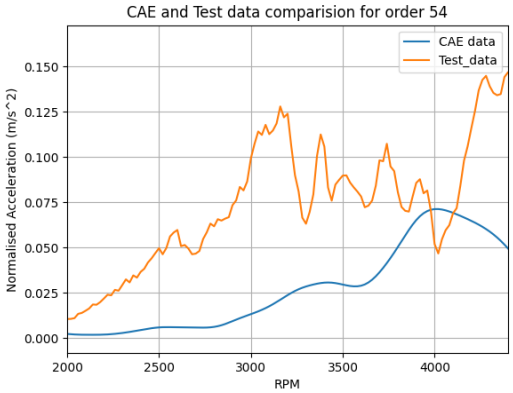

(c) Node on the electric motor

Figure A.34: Acceleration response for order 54

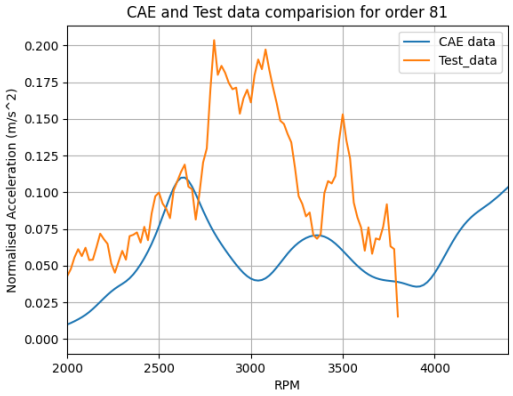

(a) Node on the top of gearbox

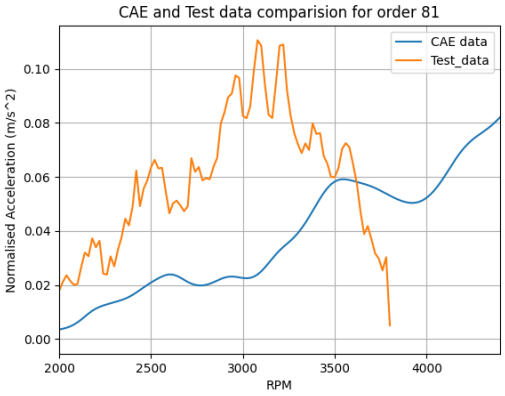

(b) Node on the side of gearbox

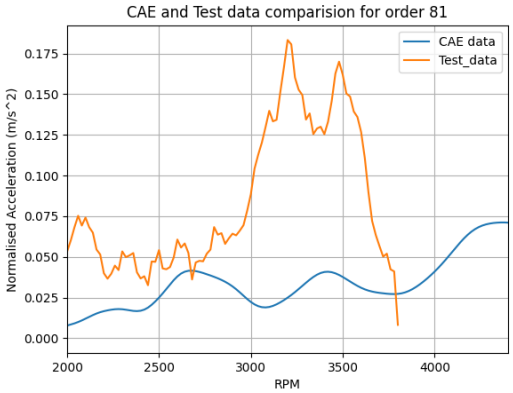

(c) Node on the electric motor

Figure A.35: Acceleration response for order 81

A.3.2.2 Electric Motor Excitation Orders

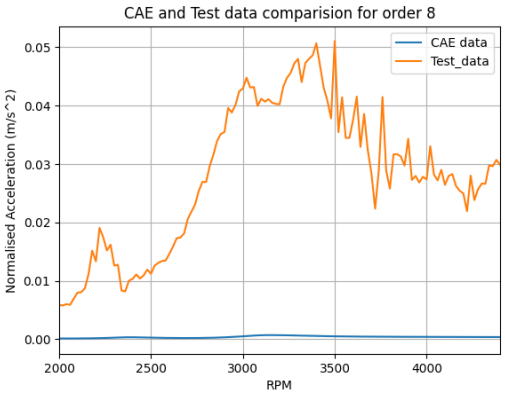

(a) Node on the top of gearbox

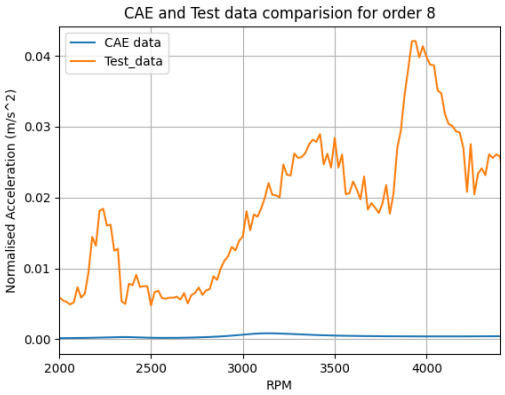

(b) Node on the side of gearbox

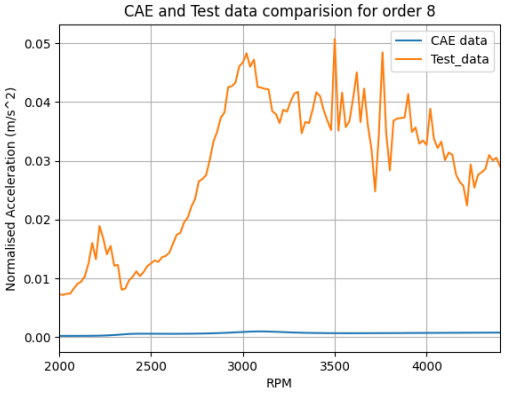

(c) Node on the electric motor

Figure A.36: Acceleration response for order 8

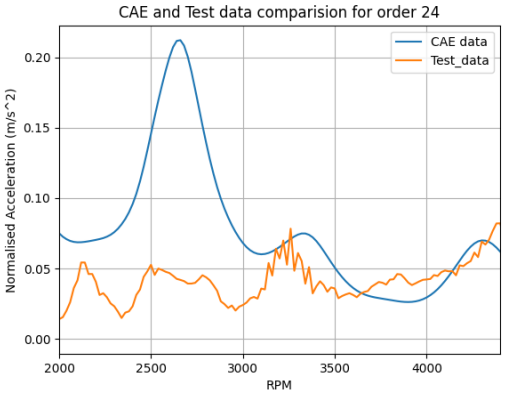

(a) Node on the top of gearbox

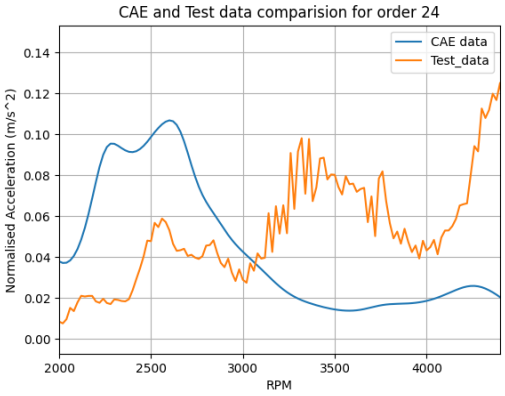

(b) Node on the side of gearbox

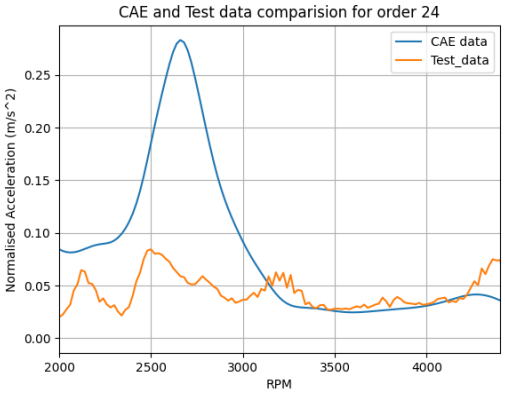

(c) Node on the electric motor

Figure A.37: Acceleration response for order 24

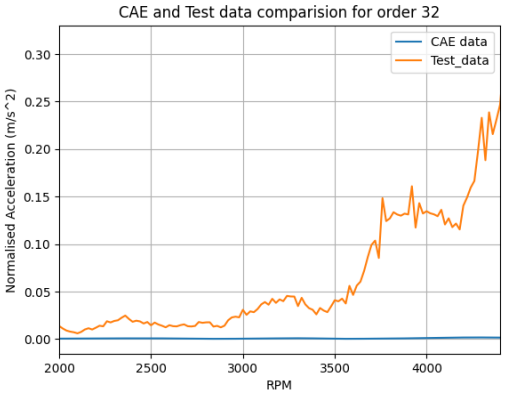

(a) Node on the top of gearbox

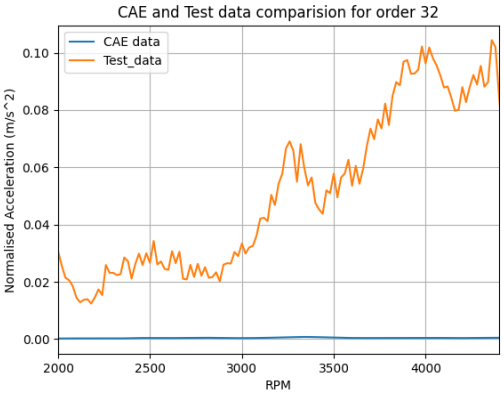

(b) Node on the side of gearbox

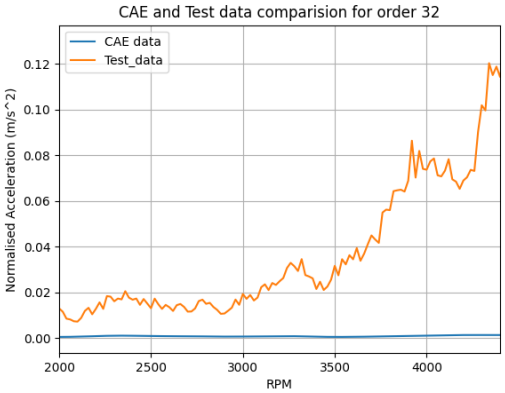

(c) Node on the electric motor

Figure A.38: Acceleration response for order 32

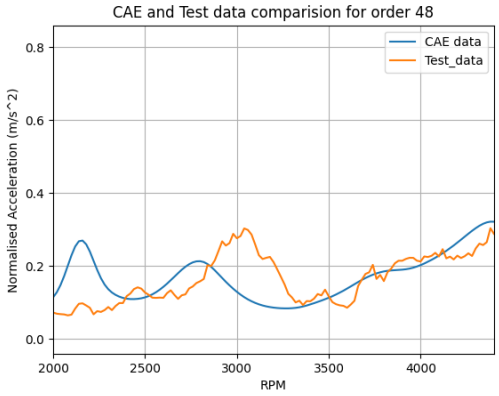

(a) Node on the top of gearbox

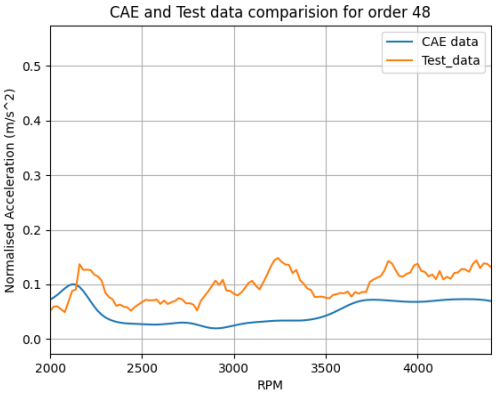

(b) Node on the side of gearbox

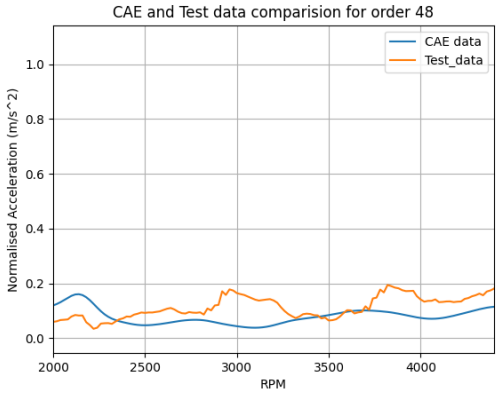

(c) Node on the electric motor

Figure A.39: Acceleration response for order 48

DEPARTMENT OF MECHANICS AND MARITIME SCIENCES
CHALMERS UNIVERSITY OF TECHNOLOGY
Gothenburg, Sweden
www.chalmers.se

CHALMERS
UNIVERSITY OF TECHNOLOGY